J. Fluid Mech. (1991), *vol.* 229, *pp.* 173–204
Printed in Great Britain

Lateral straining of turbulent boundary layers. Part 1. Streamline divergence

By SEYED G. SADDOUGHI† AND PETER N. JOUBERT
Department of Mechanical Engineering, University of Melbourne, Parkville 3052, Australia

(Received 17 July 1990 and in revised form 19 December 1990)

Extensive experimental studies are presented of the effects of prolonged streamline divergence on developing turbulent boundary layers. The experiment was arranged as source flow over a flat plate with a maximum divergence parameter of about 0.075. Mild, but alternating in sign, upstream-pressure-gradient effects on diverging boundary layers are also discussed.

It appears that two overlapping stages of development are involved. The initial stage covers a distance of about 20 initial boundary-layer thicknesses (δ_0) from the start of divergence, where the coupled effects of pressure gradient and divergence are present. In this region there is a fairly large reduction in divergence parameter, R_θ (Reynolds number based on momentum thickness) remains constant (≈ 1400) and the boundary-layer properties change rapidly. In the second region, which lasts nearly to the end of the diverging section, the pressure-gradient effects are negligible, the rate of decrease in divergence parameter is very small and R_θ increases gradually. Up to the last measurement station ($\approx 100\delta_0$) the flow is still considered to be at a low Reynolds number ($R_\theta \approx 2000$). For almost the entire length of this region, the profiles of non-dimensional eddy viscosity appear to be self-similar, but have larger values than for the unperturbed flow. Also in this region, beyond $35\delta_0$, the wake parameter, which has reduced significantly, becomes nearly constant and independent of R_θ. On the other hand the entrainment rate attains a constant value at around $50\delta_0$. It appears that the boundary layer reaches a state of equilibrium. It is suggested that this is the result of an enhanced turbulent diffusion to the outer layer. Spectral measurements show that divergence affects mainly the low-wavenumber, large-scale motions. However, there is no change in large-eddy configurations, since the dimensionless structure parameters show only negligible deviations from the unperturbed values.

1. Introduction

This investigation represents one of the complex-flow projects at the University of Melbourne – a review of some selected work on perturbed turbulent boundary layers at this laboratory has been given by Saddoughi (1989). Complex flows are defined by Bradshaw (1971) as 'shear layers with complicating influences like distortion by extra rates of strain or interaction with another turbulence field'. In simple shear flows, the basic strain rate is $\partial U/\partial y$, but in complex flows an additional shear (e.g. due to curvature, rotation, lateral straining, etc.) would be added to this. Extra-strain rates can have surprisingly large nonlinear effects on the turbulence structure of the

† Present address: Center for Turbulence Research, Stanford University, CA 94305, USA and NASA-Ames Research Center, MS 202 A-1, Moffett Field CA 94035, USA.

flow (see Bradshaw 1973). The dimensionless parameter, which defines the strength of an extra-strain rate, e, was identified by Bradshaw to be $e/(\partial U/\partial y)$, and for fairly thin shear layers, $0.01 \leqslant e/(\partial U/\partial y) \leqslant 0.1$.

It appears that the present time calculation methods cannot fully predict most of the complex flows (Bradshaw 1988), so that, to gain a better understanding and improve our prediction capabilities, we have to resort to experimentation. For experimental studies, two lines of investigation have to be adopted. Firstly, to understand their individual effects, experiments ought to be designed in such a way that each of these extra-strain rates can be studied in isolation. Secondly, since in some of the practical problems it is the combination of the extra-strain rates which affects the flow, and the available evidence (e.g. Smits & Joubert 1982) indicates that the combined influence of different perturbations is not given by a simple summation of their separate effects (see Smits & Wood 1986), it is extremely important that we also study these cases. However, apparently nowadays the research in complex flows is directed only towards the study of flows of the second type. This trend is based upon the conclusion that the individual effects of extra rates of strain are very well documented. While this conclusion may be true for streamline curvature, it is certainly not correct for lateral straining, which is one perturbation that affects most of the three-dimensional or axisymmetric shear layers.

In the usual notations the extra-strain rate due to lateral straining is equal to $\partial W/\partial z$. For example, as well as other extra rates of strain, the boundary layers over the nose and tail of a body of revolution are affected by streamline divergence ($\partial W/\partial z > 0$) and streamline convergence ($\partial W/\partial z < 0$) respectively. Flow over a cone and source flow over a flat plate are affected by 'simple divergence', where divergence remains constant through the boundary layer, but the divergence occurring on the attachment line of a swept wing is of the 'varying' type, in which divergence increases from the edge of the boundary layer to the wall (Head & Prahlad 1974). Bradshaw's (1973, 1988) reviews of the work on lateral straining showed that there were no experiments on simple divergence alone. As well, Patel & Baek (1987) indicated that there was practically no information available on the effects of lateral straining on the turbulence, and so took measurements in the turbulent boundary layer in the windward and leeward planes of symmetry of an axisymmetric body at incidence. Their results demonstrated the attenuation of turbulence, due to the effects of convergence, over the rear of the body. However, turbulence measurements could not be taken in the inner half of the boundary layer on the windward side, since the layer was very thin. This restricted their conclusions about the effects of divergence.

Our literature survey (see Saddoughi 1988) showed that, except for Sjolander (1980) who presented only mean-flow results, the only other experiment on simple divergence was that of Smits, Eaton & Bradshaw (1979*a*), where turbulence measurements for a boundary layer under the influence of concave longitudinal curvature and divergence for $R_\theta > 4000$ were taken. In the latter experiment the boundary layer was developed axially on a circular cylinder and diverged over a cone with a 40° included angle; the flow over the cone was open to the atmosphere. Consequently, transition from the circular cylinder to the conical flare took place over a concave curve. Also, the pressure gradient in the transition region was both large and changing in sign. The flared cone was short, and the most-downstream turbulence-measuring station was at 273 mm, which was only a distance of about $13\delta_0$ from the end of the concave curve. They concluded that at upstream stations the interaction between concave curvature and divergence was large and the changes

could not be totally attributed to divergence alone, but the changes at downstream stations were due to divergence.

By now it is well known that a boundary-layer response to the application or removal of curvature is a very slow process (see Smits, Young & Bradshaw 1979*b*; Gillis & Johnston 1983; Barlow & Johnston 1988). Recently, Alving, Smits & Watmuff (1990) have shown that a distance of more than $90\delta_0$ after the end of curvature will be needed for a boundary layer to recover from the effects of a strong convex curvature. As well, according to the studies of Muck, Hoffmann & Bradshaw (1985) and Hoffmann, Muck & Bradshaw (1985), this response is an order of magnitude slower for concave curvature than it is for convex curvature. Hence, based on these facts, and the extensive comparisons and analysis of data presented by Saddoughi (1988), it appears that the results for the cylinder-flare experiment, even at the most-downstream station ($\approx 13\delta_0$), are not free from the effects of strong upstream concave curvature. However, there is no doubt that the experiment of Smits *et al.* (1979*a*) gives an excellent case of the interaction problem. For example the large-scale roll cells – commonly referred to as Taylor–Görtler vortices – which are generally present in concave flows (e.g. see Smits *et al.* 1979*b*), disappeared in the cylinder-flare experiment. Smits *et al.* (1979*a*) suggested that this was apparently due to the nonlinear interaction of longitudinal vorticity and spanwise vorticity which were amplified by concave curvature and lateral divergence respectively.

The above short review indicates that for laterally strained turbulent boundary layers, extremely little broadband-turbulence data are available; there are no spectral measurements at all. The need for better understanding of the overall response of boundary layers to prolonged application of divergence alone is clear. This can be achieved by obtaining a large set of accurate experimental data, which then can enhance our understanding of the physical processes involved, and also help the development – or improvement – of turbulence models. This paper is an attempt in that direction.

Of the two methods of achieving a simple divergence – flow over a cone and source flow over a flat plate – an experimental approximation to the latter one was chosen for the present investigation, since in this case the complications arising from the effects of upstream curvature will not be present. However, here too, in order to obtain large values of the divergence parameter, the turbulent boundary layer ought to be developed in a straight section, before the lateral straining is applied. This is because, as our earlier studies showed (see Saddoughi 1988), if the turbulent boundary layer originated in the diverging section, the divergence parameter would always remain very low, which was also indicated by Smits *et al.* (1979*a*) for a boundary layer starting at the apex of a circular cone for any cone angle. Thus in our case, this change of direction of the flow (parallel-to-diverging) results in the inevitable existence of a mildly varying divergence at the start of the diverging section. It was hoped that it would vanish quickly. This part of the study is concerned mainly with developing turbulent boundary layers undergoing the effects of prolonged ($\approx 100\delta_0$) divergence. Also, as will be shown in the next section, at the upstream stations the boundary layer was affected by mild, but alternating in sign, pressure gradients. Consequently, some of the present experiments were devoted to the investigation of the effects of these pressure gradients on diverging boundary layers. In Part 2 the effects of convergence on fully developed turbulent boundary layers will be studied. It should be emphasized that a great deal of time and effort have been spent on obtaining accurate and repeatable results.

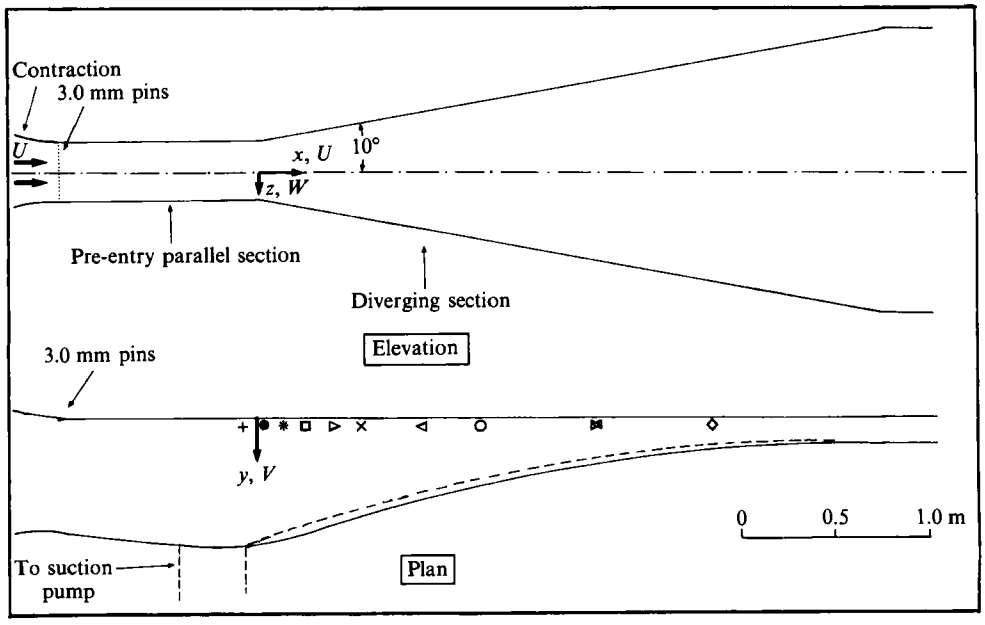

FIGURE 1. Details of the test sections. Solid line for layer A; dashed line indicates the changes needed for layer B. The stations for hot-wire measurements are shown with the symbols used.

2. Apparatus and measurement techniques

The wind tunnel was an open-return blower type. During the manufacture of the tunnel a number of design rules given by Mehta & Bradshaw (1979) were used. The construction details of this tunnel, as well as a more detailed description of the measurement techniques, are given by Saddoughi (1988). Results for two sets of experiments are reported here. The corresponding boundary layers of these experiments are called layer A and layer B. The turbulent boundary layers were developed in a pre-entry parallel section for nearly 1050 mm, before the lateral straining was applied. Streamline divergence was achieved by diverging two sidewalls, while measurements were taken on a straight third wall continuous with the entry section. The total included angle of divergence was 20° (figure 1). The divergence, D, at any point on the plane of symmetry of the flow is equal to $1/(x-x_0)$, where x_0 is the longitudinal distance from the start of the diverging section to the virtual origin of the divergence. D is positive for a divergent flow and negative for a convergent flow. The divergence value at the start of the diverging section was 11.4×10^{-4} mm^{-1} which dropped to 2.4×10^{-4} mm^{-1} by the end of the section. The pressure gradient, over the entire working section, was adjusted by a variable curved fourth wall opposite to the straight third wall. As shown in figure 2, for layer A, a nominally zero pressure gradient was achieved in both the parallel and the diverging sections, except at the transition part (parallel-to-diverging) where this was not possible. At the end of the parallel section and at the start of the diverging section, the pressure-gradient parameters, $(\delta^*/\tau_w)\,\mathrm{d}p/\mathrm{d}x$, were about -0.30 and 0.34 respectively, which are considered to be fairly mild since $|(\delta^*/\tau_w)\,\mathrm{d}p/\mathrm{d}x| < 0.5$ (Bradshaw & Unsworth 1974). For layer B the experimental arrangement was the same as that for layer A, but just upstream of the transition section a suction slot was cut out on the opposite wall to that where measurements were taken (see figure 1).

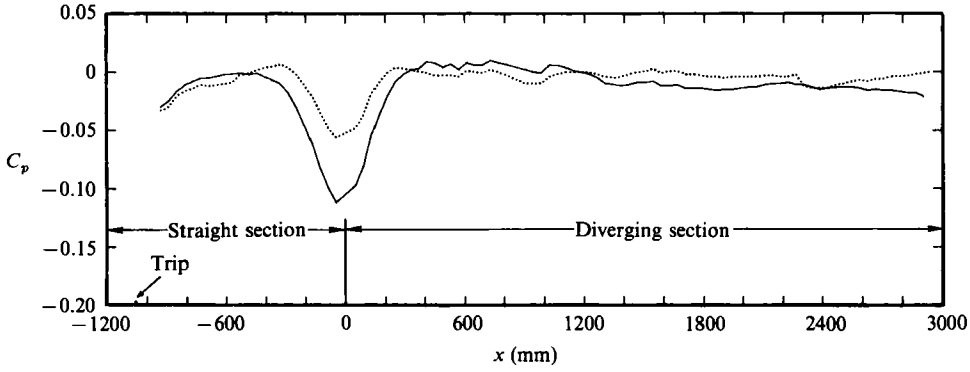

FIGURE 2. Wall-pressure distribution C_p: ——, layer A; ....., layer B.

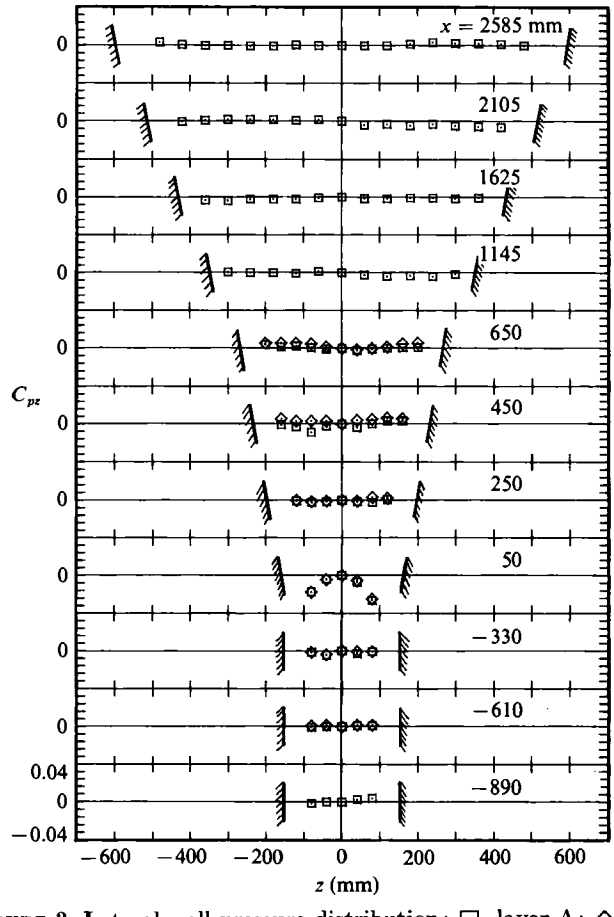

FIGURE 3. Lateral wall-pressure distribution: ⊡, layer A; ◇, layer B.

The amount of suction and the shape of the curved wall were adjusted such that the pressure-gradient jump at the transition section of this layer was halved compared with that for layer A (figure 2). In this case, in the adverse-pressure-gradient region, $(\delta^*/\tau_w)\,\mathrm{d}p/\mathrm{d}x$ reduced to 0.21. This allowed the effects of a change in pressure gradient to be evaluated. For both layers, the variation of lateral-wall-pressure

distribution for the rest of the tunnel was negligible (figure 3), except at the transition section, which indicates that reasonably two-dimensional flows were achieved.

For both experiments, boundary-layer transition was achieved by means of round stimulator pins which had both height and diameter of 3.0 mm and were placed at 80 mm downstream of the contraction outlet with a spanwise spacing of 9.0 mm.

Pressure differences were measured by means of an electronic manometer (Datametrics Barocel Model 1014 A). Measurements were taken at a constant unit Reynolds number ($U_R/\nu = 0.53 \times 10^6$ m^{-1}) which corresponded to a nominal reference velocity (U_R) of 8 m s. The free-stream turbulence intensity was 0.2%. Reference velocities were measured by means of a Pitot-static probe which was placed at the contraction outlet. Mean-velocity profiles were taken with a round Pitot probe with an outside diameter of 0.73 mm. The flow angles were measured with a three-tube Conrad probe in null mode. Coles' (1962) method was used to analyse the velocity profiles. The values of the wake parameter, Π, were obtained by fitting the data to a log-law line with constants $\kappa = 0.41$ and $C = 5.0$, since Coles used those constants. Skin-friction coefficients were obtained by reprocessing the velocity-profile data using Coles's method, but this time the constants used were $\kappa = 0.41$ and $C = 5.2$. These are the constants suggested by de Brederode & Bradshaw (1974). Skin-friction coefficients were also found by applying Patel's (1965) calibration to Preston-tube measurements. The Preston tubes were made from hypodermic tubing of outside diameter 1.25 mm.

The hot-wire instrumentation and calibration techniques used were all similar to those described by Perry (1982). Normal (single-sensor DISA 55 P05) and crossed (dual-sensor DISA 55 P51) hot-wire probes in conjunction with home-made constant-temperature anemometers were used for turbulence measurements. Wollaston wires were soldered to the above sensors and they were etched till the platinum core filament, which had a diameter of 5 μm, was reached. The active lengths were approximately 1.0 mm. The crossed wires were nominally at ±45° to the mean-flow direction. All the hot wires were operated with a nominal resistance ratio of 2.0. Dynamic calibration techniques were used to calibrate all the hot wires; crossed wires were dynamically matched prior to the calibration. The square-wave response of the anemometers was adjusted for optimum damping and their frequency response was close to 20 kHz. Hot-wire signals were low-pass filtered (Krohn-Hite model 3321) at 30 Hz and 10 kHz, during calibration and turbulence-profile measurements respectively. The signals were sampled on-line by a PDP 11/10 digital computer using a 12-bit analog-to-digital convertor. The calibration was checked before and after each profile measurement. Whenever the drift in hot-wire signals was more than ±2% the profile was repeated. For each point in a turbulence profile, four sets of 8000 samples at a sampling frequency of 200 Hz were taken. These data were stored on magnetic tapes and later reduced later. The reduction programme evaluated mean velocities and turbulence quantities up to quadruple products.

The spectral-measurement techniques were the same as those outlined by Perry, Lim & Henbest (1987). Uncalibrated hot wires were used for spectral measurements. The u-spectra were measured with a normal hot wire and v- and w-spectra with dynamically matched crossed hot wires. The power-spectral densities in energy per unit streamwise wavenumber, k_1, of u-, v- and w-fluctuations, which represent the distribution of turbulent energy among the different eddy scales, are given by $\Phi_{11}(k_1)$, $\Phi_{22}(k_1)$, and $\Phi_{33}(k_1)$ respectively. The spectral densities of the hot-wire signals were found by means of a digital computer which used a fast-Fourier-transform

algorithm. Using Taylor's hypothesis of frozen turbulence, k_1 was inferred to be equal to $2\pi f/U_c$, where U_c, the local convection velocity, was assumed to be equal to the local mean velocity at a given point in the flow. To improve the frequency bandwidth of the spectrum at low frequencies, the signal was sampled at three different sampling rates. The signal was low-pass filtered at half the sampling rate to avoid aliasing. Overall, the resulting frequency bandwidth was 0.1 Hz to 10 kHz. A single spectral file was obtained by joining the above three files. This file was smoothed and normalized such that

$$\int_0^\infty \Phi_{11}(k_1)\,\mathrm{d}k_1 = \overline{u^2}, \tag{1}$$

and likewise for v- and w-fluctuations.

It is well known that some difficulties exist in obtaining accurate measurements of Reynolds stresses close to the wall (see Willmarth & Bogar 1977; Willmarth & Sharma 1984). However, Ligrani & Bradshaw (1987), concluded, based on extensive experimental investigations, that adequately accurate measurements up to the quadruple products of the longitudinal velocity fluctuations near the wall can be taken with a normal hot wire which has an active length (spanwise extent) of about 20–25 viscous lengthscales (ν/U_τ) and a length-to-diameter ratio of about 200. All the hot wires used for taking measurements at all the stations of both layers A and B satisfied the criteria given by Ligrani & Bradshaw.

To establish that the upstream unstrained turbulent boundary layer was close to a normal state (in Coles' sense), for layer A at $x = -410$ (all the x measurements are in mm), which was a station in the straight section and the pressure gradient was nominally zero, a mean-velocity profile was taken by the Pitot probe. The measured value of the wake parameter at this station and that given by Coles for the same R_θ were very close. As well, at this station three broadband-turbulence profiles (one with the normal hot wire and the other two with crossed hot wires in UV- and UW-modes) and families of spectra for u, v and w were measured. Saddoughi (1988) has shown that these results agree excellently with the zero-pressure-gradient low-Reynolds-number plane-flow data of Erm (1988) (hereafter referred to as the plane-flow data) for approximately the same R_θ as the present investigation. Furthermore, Saddoughi (1988) has shown that at a typical station in the diverging section the longitudinal mean-velocity profiles, which were measured by four different means (Pitot probe and hot-wires), collapsed, and also that the profiles of r.m.s. velocity fluctuations in the streamwise direction obtained by the different hot wires agreed excellently with each other. At this station for the points close to the wall, all these agreements were better than $\pm 2\%$.

Thus, based on the forgoing discussion, it was concluded that the present experimental results contain accurate sets of measurements for low-Reynolds-number flows with streamline divergence. All these data are available on floppy discs.

3. Results and discussion

3.1. *Mean flow*

Figure 4 shows the local skin-friction coefficients, $C_f = \tau_w/(0.5\rho U_e^2)$, and these are compared with the plane-flow data. The C_f measured in the parallel section for both layers A and B, and the plane-flow data collapsed well up to $x \approx -400$. In the pressure-jump region they deviated from the plane-flow data. The rise in C_f values at the end of the straight section and their subsequent fall at the beginning of the diverging section are the effects of favourable and adverse pressure gradients

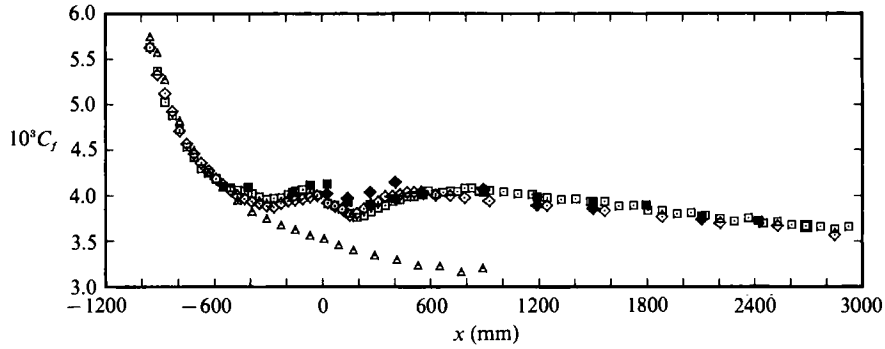

FIGURE 4. Skin-friction coefficient, $C_f = \tau_w/(0.5\rho U_e^2)$, Preston-tube measurements (the solid symbols are deduced from logarithmic law); ⊡, layer A; ◇, layer B; △, plane-flow data at 8 m/s (Erm 1988).

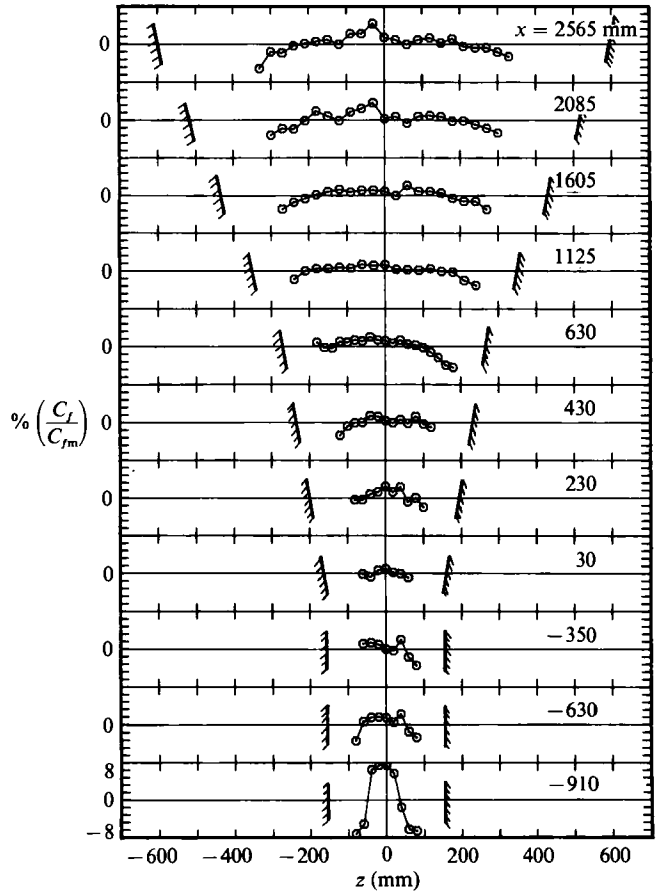

FIGURE 5. Lateral variation of C_f for layer A. Results normalized with the mean value.

respectively. The second rise in C_f which took place in the diverging section was due to the effects of divergence. In general the agreement between the C_f values obtained from Preston-tube measurements and those deduced from logarithmic profiles were within about 2.5%, except for the profile at $x = 25$ for layer A. The lateral variations of C_f for layer A, non-dimensionalized with the mean value across the measured

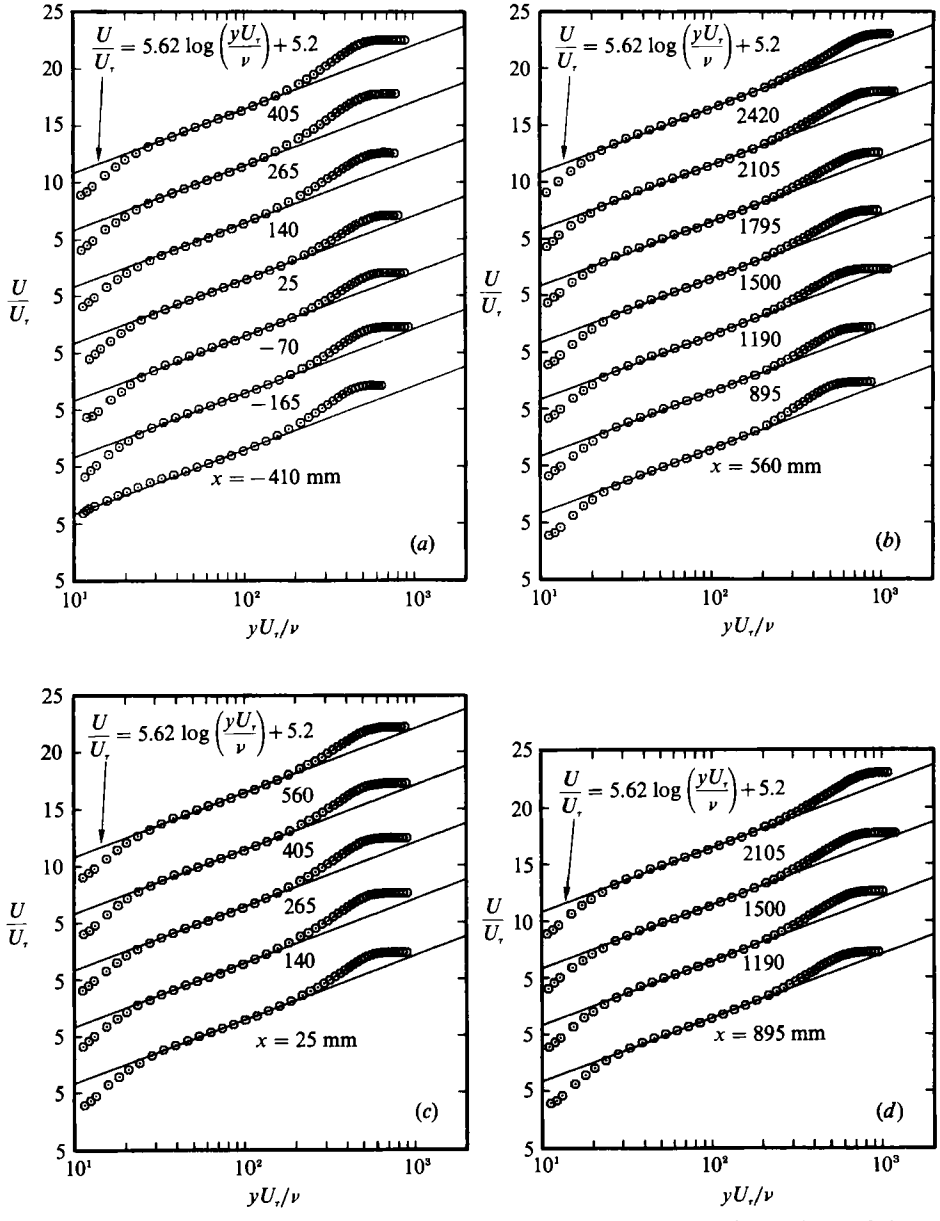

FIGURE 6. Centreline mean-velocity profiles (semi-log plot); (*a*, *b*) layer A; (*c*, *d*) layer B.

region, are shown in figure 5. These results correspond to readings from Preston tubes located at 20 mm intervals in the spanwise direction. This spanwise distance between the measurement points was about 0.99 and 0.54 times the boundary-layer thicknesses at $x = -410$ and 2420 respectively. The spanwise variations for the central half of the span were mostly about $\pm 2\%$, except at $x = -910$ which was very near to the tripping device, where the variation was about $\pm 10\%$. The slight drops in lateral values of C_f which generally occurred at z-positions beyond the central half of the span (mostly at downstream stations) were probably due to the effects of corner flows.

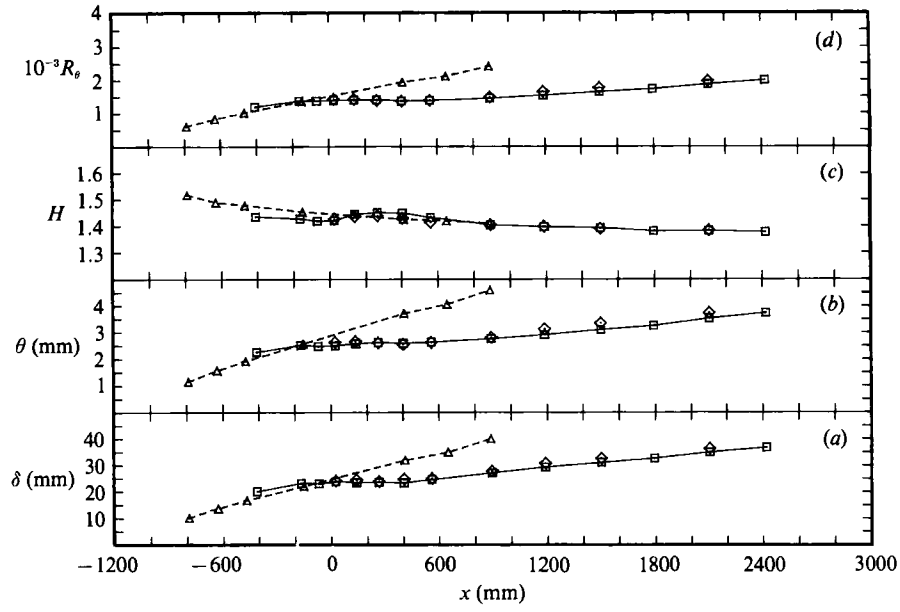

FIGURE 7. Integral parameters: (*a*) boundary-layer thickness, δ; (*b*) momentum thickness, θ; (*c*) shape parameter, H; (*d*) momentum-thickness Reynolds number, R_θ. For key to symbols see figure 4.

		U_e/U_R		δ (mm)		δ^* (mm)		θ (mm)		R_θ	
x (mm)	Symbol	layer A	layer B	layer A	layer B	layer A	layer B	layer A	layer B	layer A	layer B
−70	+	1.052	—	23.11	—	3.51	—	2.48	—	1373	—
25	●	1.052	1.027	23.84	24.16	3.55	3.75	2.50	2.63	1395	1429
140	*	1.024	1.008	23.50	24.50	3.72	3.82	2.58	2.66	1400	1433
265	⊡	1.003	0.998	23.56	23.91	3.80	3.74	2.62	2.60	1410	1385
405	▷	0.996	1.000	23.36	24.79	3.75	3.64	2.59	2.55	1370	1370
560	×	0.998	1.005	24.64	25.12	3.76	3.73	2.63	2.62	1385	1389
895	◁	0.999	1.004	27.10	27.83	3.90	3.95	2.77	2.81	1455	1493
1190	⊙	1.000	1.000	29.30	30.74	4.07	4.37	2.91	3.12	1540	1655
1795	⋈	1.007	—	32.70	—	4.49	—	3.25	—	1725	—
2420	◇	1.007	—	36.78	—	5.15	—	3.74	—	1993	—

TABLE 1. Mean-flow parameters and symbols at the stations for hot-wire measurements

Figure 6 shows semi-logarithmic plots of the mean-velocity profiles. All the profiles had extensive logarithmic regions. Profile shapes were normal and no apparent distortion of them could be detected. As shown by Saddoughi (1988), the above observations were also true for the off-centreline profiles which were measured for layer A. Integral parameters are shown in figure 7, where they are compared with the plane-flow data. Some of these parameters, which are for the stations where turbulence measurements were taken, are also given in table 1. For the present investigations, boundary-layer thickness $\delta(\equiv \delta_{995})$, θ and R_θ remained nearly constant for a distance of about $20\delta_0$ downstream of the start of the diverging section. Further downstream the growth rates of these parameters were much lower than for the

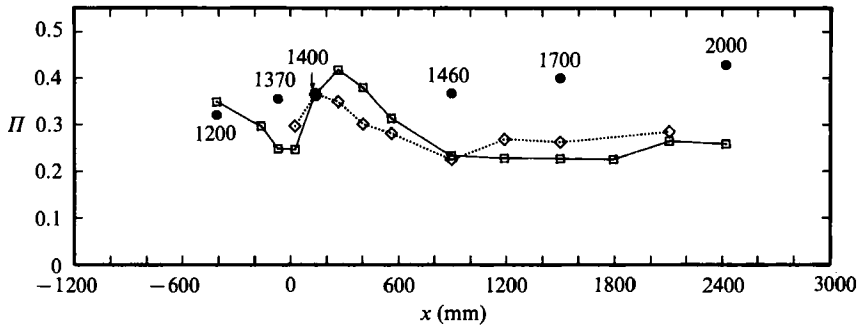

FIGURE 8. Variation of wake parameter, Π, with x. ●, Coles (1962) for the Reynolds numbers indicated; ⊡, layer A; ◇, layer B.

plane-flow case. These are due to the kinematic effects of divergence, as presented by the divergence term in the momentum-integral equation for simple-divergence layers, which is given by Kehl (1943) and Head & Patel (1968) as

$$\frac{\mathrm{d}\theta}{\mathrm{d}x} = \frac{C_f}{2} - (H+2)\frac{\theta}{U_e}\frac{\mathrm{d}U_e}{\mathrm{d}x} - D\theta. \tag{2}$$

The values of the wake parameter are plotted against x in figure 8, together with the Π values from Coles (1962) corresponding to almost the same R_θ as the present cases. The changes in Π values at the transition section are apparently due to the effects of pressure gradients. Further downstream, from $x = 265$ to 895, R_θ remained fairly constant, but Π values reduced and these low values were maintained for the rest of the diverging section even after R_θ increased gradually. These low values of Π were due to the effects of divergence. Apparently, beyond $x \approx 35\delta_0$ the boundary layer reaches a state of equilibrium and Π becomes nearly constant and independent of R_θ, which possibly indicates that the wake parameter is correlated with the rate of strain due to divergence (V. C. Patel, private communication).

The divergence can be related to the local flow velocities and angles as

$$D = \frac{1}{U}\frac{\partial W}{\partial z} = \frac{\partial \beta}{\partial z}, \tag{3}$$

where β is the flow yaw angle (Head & Prahlad 1974). Flow angles measured for layer A are shown in figure 9. These profiles serve two purposes. Firstly, they show whether the simple-divergence assumption is valid and, secondly, from these profiles divergence can be calculated and compared with the designed value which was obtained purely from the geometry of the diverging section. From figure 9 it can be seen that at each measurement station along the tunnel centreline, cross-flow was nearly zero. Also, for the off-centreline profiles, the flow angles remained nearly constant right through the layer, except at $x = 55$ and 155 where the flow angles near the wall were larger than those in the free stream. Recall that at $x = 50$ there were also variations in lateral-wall-pressure coefficients, but no appreciable changes in spanwise values of C_f were detected. It can be concluded that for the rest of the tunnel the boundary layer was affected by simple divergence, except at the transition section where the divergence varied mildly through the layer. The consequence of varying divergence near the wall and also the accuracy of divergence measurements, with respect to momentum balance, are discussed below.

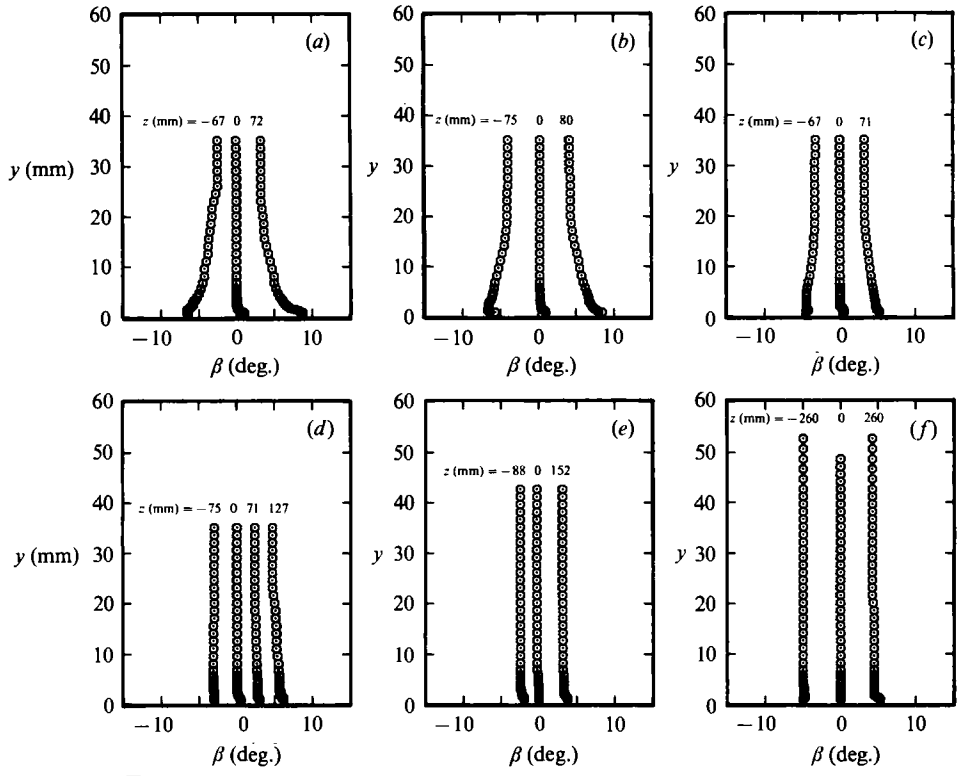

FIGURE 9. Yaw-angle profiles for layer A: (*a*) $x = 55$ mm; (*b*) 155; (*c*) 268; (*d*) 540; (*e*) 1325; (*f*) 2230.

The momentum equation (2) can be rewritten such that divergence is the only unknown. The divergence values calculated using three independent methods, namely (i) geometry of the working section, (ii) flow-angle measurements and (iii) balance of momentum can now be compared with each other. The results obtained using the above three methods for layer A are shown in figure 10. In this figure divergence values calculated using the momentum equation for layer B are also presented. Everywhere in the diverging section divergence values at mid-layer calculated from the flow-angle measurements collapsed reasonably well with the designed values, except at $x = 155$ where the measured value was higher than the designed one. Hence, it appears that the flow-angle measurements were of acceptable accuracy. Also, the momentum balances in the diverging section were mostly better than 4% of C_f, except at the upstream stations ($x = 25$ to 155), where divergence values calculated from the momentum equation were higher than those obtained from both the mid-layer flow-angle measurements and also the designed curve. These imbalances were about 22% of C_f. It may be noted that the use of the momentum equation for calculation of divergence involves an uncertainty which is associated with the fact that the gradients with respect to x for data points spaced widely apart are included in this equation. However, most of the upstream momentum imbalances reflect the effects of varying divergence, and show that the growth rates of momentum thickness at these two stations apparently correspond to divergence values which were intermediate between the mid-layer and wall values. As expected, for layer B in the diverging section, divergence calculated from the momentum equation had almost the same values as those for layer A.

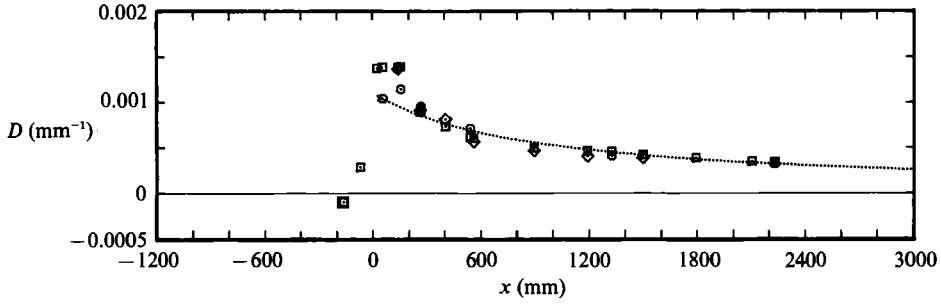

FIGURE 10. Divergence, D: ....., from tunnel geometry; ⊡, from momentum balance for layer A; ◇, from momentum balance for layer B; ⊙, measured at mid-layer for layer A.

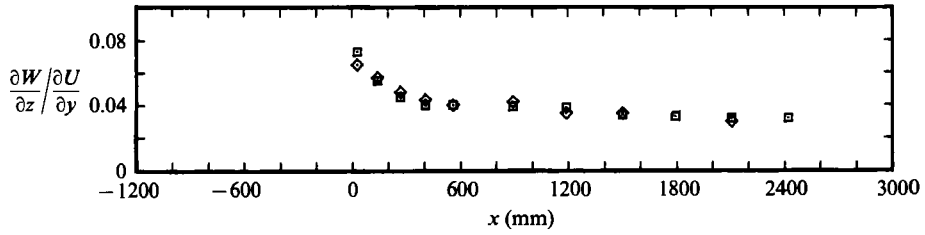

FIGURE 11. Divergence parameter, $(\partial W/\partial z)/(\partial U/\partial y)$, at mid-layer: ⊡, layer A; ◇, layer B.

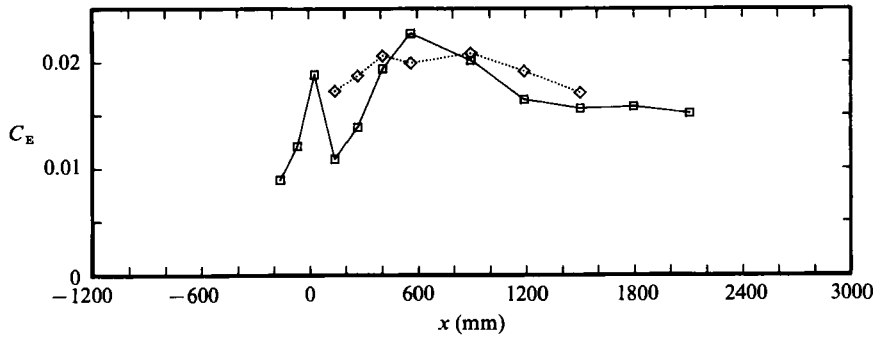

FIGURE 12. Entrainment rate, $C_E = V_E/U_e$: ⊡, layer A; ◇, layer B.

The divergence parameter is defined as $(\partial W/\partial z)/(\partial U/\partial y)$. The values for this parameter, which were calculated from the designed values of divergence and the velocity-profile measurements in the mid-layers, are shown in figure 11. For layer A at $x = 25$, the divergence parameter was equal to 0.073, which is a fairly large value. At the downstream stations the rate of decrease of this parameter with streamwise distance was very small.

Head & Patel (1968) proposed that the entrainment rate for a laterally strained layer is given by

$$C_E = \frac{1}{U_e}\frac{d}{dx}[U_e(\delta-\delta^*)]+D(\delta-\delta^*). \tag{4}$$

Entrainment rates are plotted in figure 12. As expected from the formulation of C_E, this figure indicates both the effects of the change-in-pressure-gradient jump on the entrainment rate as well as the increase in C_E due to divergence (Head 1976, Crabbe

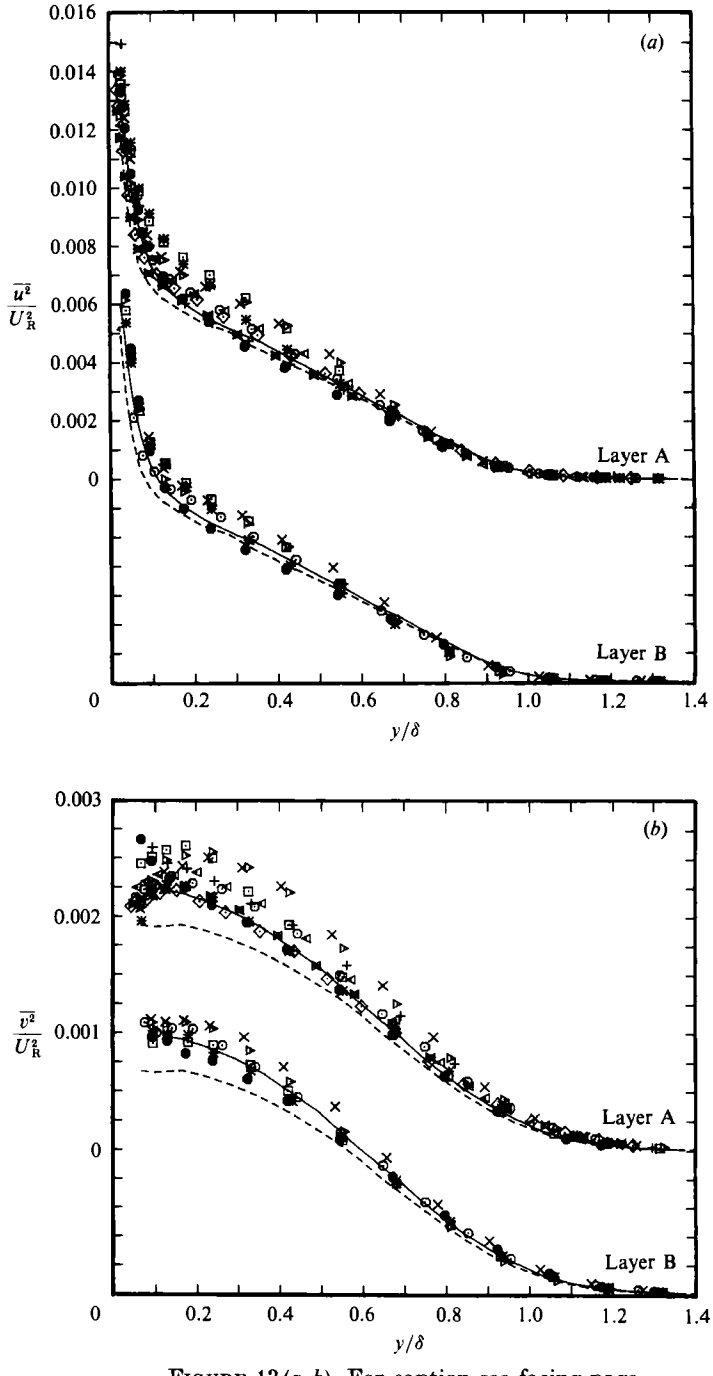

FIGURE 13 (a, b). For caption see facing page.

1977 and Sjolander 1980 have also discussed the effects of lateral straining on the entrainment rate). For the present experiments, C_E values for the downstream stations, $x > 50\delta_0$, became independent of R_θ and attained a constant value. However, it appeared that even in this equilibrium region, Head's (1958) original

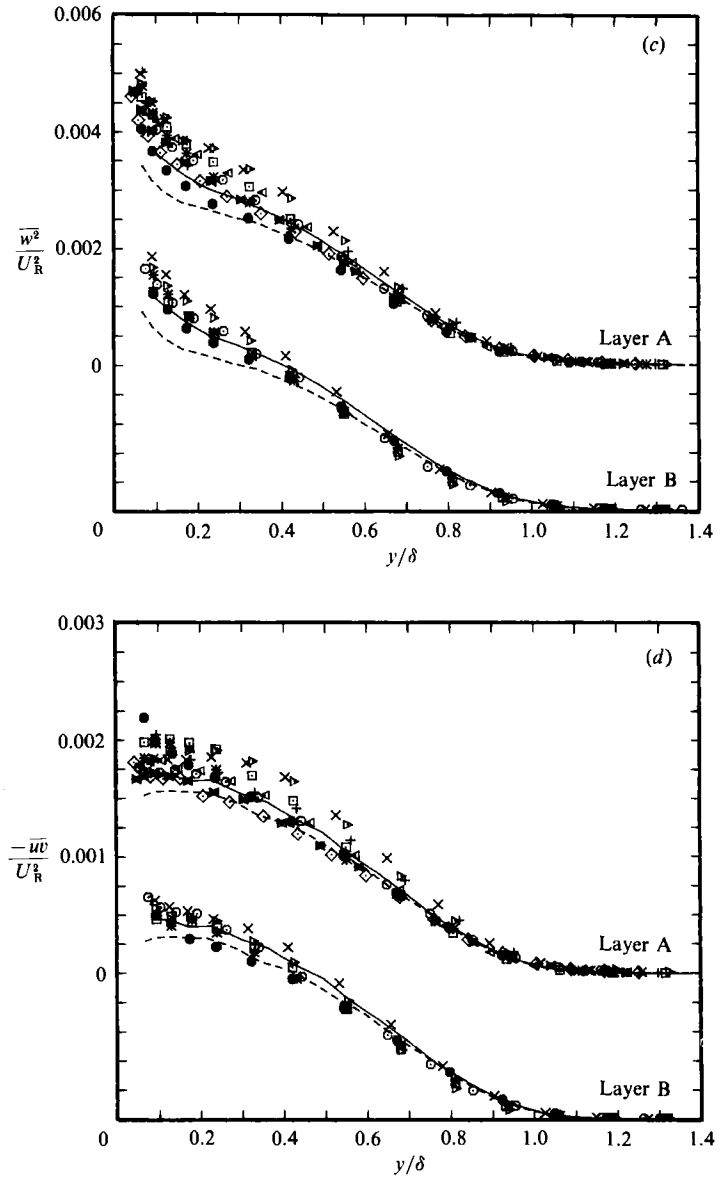

FIGURE 13. Profiles of Reynolds stresses: (*a*) $\overline{u^2}/U_R^2$; (*b*) $\overline{v^2}/U_R^2$; (*c*) $\overline{w^2}/U_R^2$; (*d*) $-\overline{uv}/U_R^2$. ——, $R_\theta = 1565$ and – – –, $R_\theta = 2180$ from Erm (1988). For key to other symbols see table 1.

auxiliary equation, which is $C_E = F[(\delta - \delta^*)/\theta]$, where the form of the empirical function F is specified by him, did not satisfy the present data.

3.2. *Broadband turbulence*

3.2.1. *Reynolds stresses and triple products*

All the turbulence quantities measured are for the plane of symmetry of each layer. The normalized profiles of Reynolds normal stresses ($\overline{u^2}/U_R^2, \overline{v^2}/U_R^2, \overline{w^2}/U_R^2$) and the shear stress, $-\overline{uv}/U_R^2$, are shown in figure 13. The profiles for these stresses, and almost all the other broadband-turbulence results of the present experiments, have

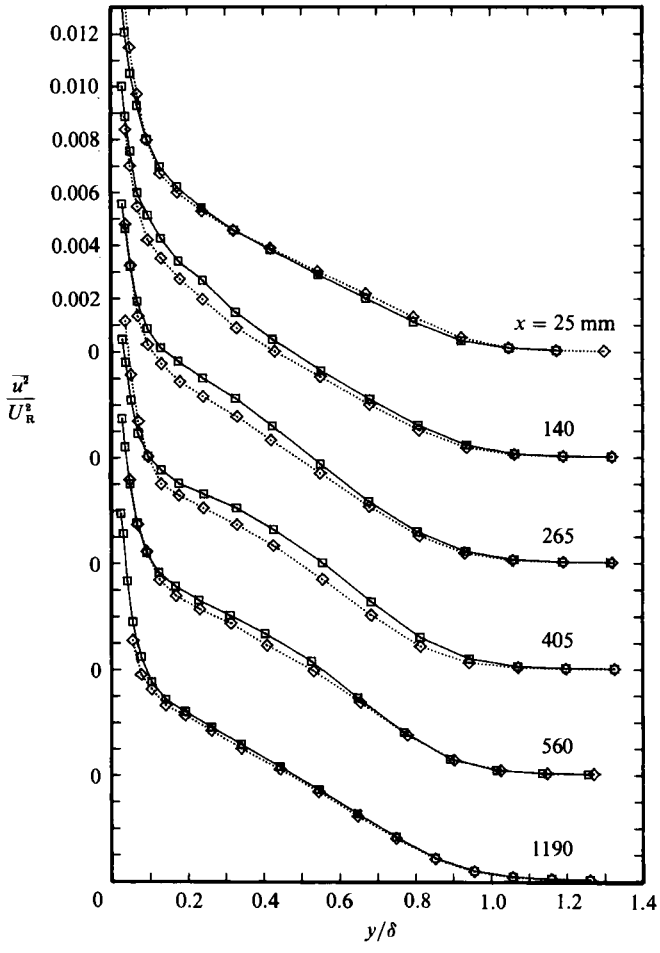

FIGURE 14. Comparison between layer A (⊡) and layer B (◇) showing the effects of the change-in-pressure-gradient jump on the profiles of $\overline{u^2}/U_R^2$ at each measurement station.

been compared with the plane-flow data of Erm for $R_\theta = 1565$ and 2180. For layer A, for the region from the start of the diverging section to approximately $x = 560$ where R_θ remains constant, the stresses at a fixed y/δ (for $y/\delta \approx 0.2$ to 0.5) appear to increase gradually with streamwise distance and they are higher than the plane-flow data for $R_\theta = 1565$. This could be due to the effects of divergence and pressure gradients. The stresses for $x = 405$ to 560 ($\approx 20\delta_0$) have reached their maximum values in layer A before they gradually decrease with increase in x. While Reynolds shear stresses drop back to the plane-flow data for $R_\theta = 2180$, the normal stresses obtain values which are slightly higher than those corresponding to the plane-flow case. The above reduction in the values of the stresses with streamwise distance are apparently due to the effects of the increase in R_θ (see Murlis, Tsai & Bradshaw 1982; Erm 1988) and the slight decrease in divergence parameter. For layer B, where the strength of the upstream pressure gradient was lower than that of layer A, the above trends are also present, but the increase in the stress levels are rather small.

If the profiles for layer A are compared with those for layer B, then the effects of the change-in-pressure-gradient jump on the developing boundary layers which have

the same divergence parameters and also the same Reynolds number can be identified. As an example of this, the profiles of $\overline{u^2}/U_R^2$ for layer A are compared with those for layer B in figure 14. It can be observed in this figure – and also from the comparisons done for the other Reynolds stresses, which are not shown here – that as the two layers developed along the diverging section, the differences between the values of the stresses caused by the change-in-pressure-gradient jump apparently started to propagate from the inner layer towards the edge of the boundary layer. Only around $x = 560$ to 1190 do these differences almost disappear, which apparently shows that the recovery of the boundary layer from the effects of alternating-in-sign upstream pressure gradients is a slow process. These results are in accordance with the well-known effects of pressure gradients, that a change in pressure gradient affects the velocity gradient and turbulent stresses immediately in the inner layer, and the response of turbulence in the outer layer to a change in pressure gradient is slow (see Smits & Wood 1985; Bradshaw & Ferriss 1965). The present data suggest that the increases in the values of the stresses in the outer layer of layer A, where in general the effects of the extra-strain rates are maximum, cannot be totally attributed to the effects of divergence. Therefore it has been demonstrated here that for low-R_θ boundary layers the effects of divergence on the Reynolds stresses are apparently not that large, even with the divergence parameters as high as those for the present investigations. While it appears that the effect on the Reynolds shear stress is small, among the normal stresses the maximum effect is felt by the longitudinal component: around the mid-layer of layer B at a streamwise distance of about $20\delta_0$, $\overline{u^2}/U_R^2$ has increased only by about 15%, compared with plane-flow data for the same R_θ as the present case.

Physically, the triple products of velocity fluctuations show turbulent transport of Reynolds stress by the large eddies, and they appear in the 'diffusion' parts of the transport equations. Some triple products ($\overline{u^3}, \overline{uv^2}, \overline{uw^2}, \overline{u^2v}, \overline{v^3}$) were measured and presented by Saddoughi (1988), but for brevity they will be discussed here only in terms of the derived quantities for modelling. However, it should be mentioned that divergence enhanced the triple products more significantly than the Reynolds stresses (for further discussion see §4).

3.2.2. *Derived quantities and their implications for modelling*

Any changes that the perturbations produce in dimensionless properties of the boundary layers indicate the effects on the structure of turbulence. The structural parameter $a_1 = -\overline{uv}/\overline{q^2}$, which represents the efficiency of maintenance of shear stress (Smits *et al.* 1979*b*), is one of the empirical inputs to the calculation method of Bradshaw, Ferriss & Atwell (1967) ($\overline{q^2}$, which is equal to $\overline{u^2}+\overline{v^2}+\overline{w^2}$, is twice the total turbulent kinetic energy). Based on the assumption of structural similarity, this parameter is taken to be a constant of about 0.15 in undistorted turbulent shear flows. Figure 15 shows the profiles of a_1. The low-R_θ plane-flow data indicate values close to 0.16 for this parameter around the mid-layer. In layer A, a_1 values around the mid-layer vary between 0.16 to 0.14 from the start to the end of the diverging section respectively (except at $x = 140$ where the values are close to 0.14). In layer B the values at all the stations are very close to 0.145. The shear-stress correlation coefficient, $R_{uv} \equiv -\overline{uv}/(\overline{u^2}\,\overline{v^2})^{\frac{1}{2}}$, which gives a measure of the efficiency of turbulent mixing (Murlis *et al.* 1982), is shown in figure 16. Murlis *et al.* reported that the values at $y/\delta = 0.6$ were 0.42, 0.45 and 0.40 at $R_\theta = 791$, 1900 and 4750 respectively. The values of R_{uv} for Erm's experiments around the mid-layer are about 0.5 for $R_\theta = 1565$ and 2180. For the present cases, the streamwise development of the correlation

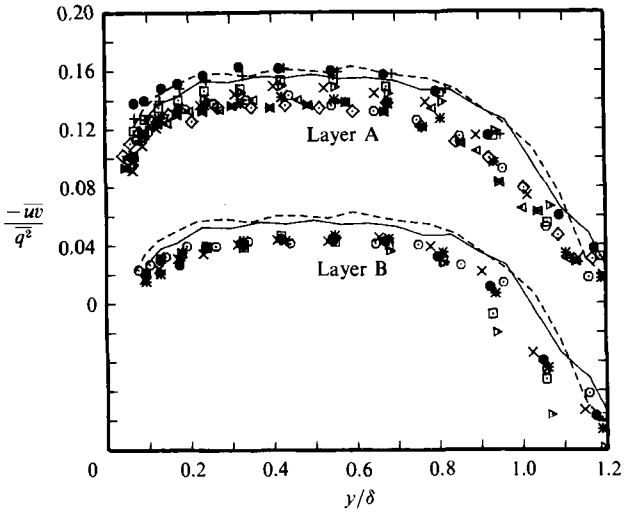

FIGURE 15. Ratio of shear stress to (twice) turbulent kinetic energy, $-\overline{uv}/\overline{q^2}$. For key to symbols see table 1 and figure 13.

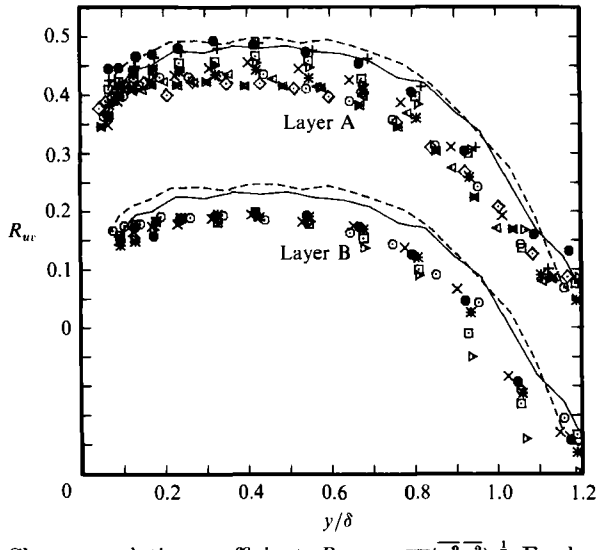

FIGURE 16. Shear-correlation coefficient, $R_{uv} \equiv -\overline{uv}(\overline{u^2}\,\overline{v^2})^{-\frac{1}{2}}$. For key to symbols see table 1 and figure 13.

coefficient in each layer is very similar to the behaviour of a_1. For layer B, an almost constant value of about 0.45 for R_{uv} can be observed for all the stations in the diverging section. The general expectation is that, as a result of the destabilizing effect of divergence, the anisotropy parameters may increase. On the contrary, compared with the plane-flow data for the same R_θ, they have – if anything – reduced, since divergence increased the normal stresses more than the shear stress. However, divergence effects on these parameters are so small that the changes can be totally neglected in the prediction methods.

Eddy-viscosity, $\epsilon_m = -\overline{uv}/(\partial U/\partial y)$, and mixing-length, $l = (-\overline{uv})^{0.5}/(\partial U/\partial y)$, concepts have been used successfully in calculation methods for self-preserving flows, but these simple concepts fail in more complicated cases like complex flows. This is

because in flows where the rate of strain changes rapidly, the Reynolds stress will respond slowly and not at once as implied by eddy-viscosity formulae (Bradshaw 1972). Over the major part of the outer layer of a zero-pressure-gradient boundary layer at high Reynolds number, the standard values of l/δ and non-dimensional eddy viscosity, $\epsilon_m/U_e\delta^*$, are 0.08 and 0.017 respectively (Cebeci & Smith 1974). In the inner layer ϵ_m and l vary linearly with distance from the wall. As shown by their formulations, eddy viscosity and mixing length are not true turbulence parameters. Therefore, for example an increase in ϵ_m and l compared with self-preserving values which is caused by a perturbation is not necessarily the consequence of an increase in Reynolds shear stress alone, but it could also be the result of a decrease in $\partial U/\partial y$ (see e.g. Hoffmann *et al.* 1985). The perturbations affecting the present flows are known to influence the behaviour of these parameters (for low-R_θ flows see Murlis 1975; Inman & Bradshaw 1981; Erm 1988, for pressure-gradient effects see Bradshaw & Ferris 1965; Galbraith & Head 1975; Head 1976; Cutler & Johnston 1989, and for experiments on lateral straining see Patel, Nakayama & Damian 1974; Crabbe 1977; Smits *et al.* 1979*a*; Sjolander 1980; Patel & Baek 1987).

The profiles of l/δ are shown in figure 17. Near the wall the effects of extra-strain rates are small and the mixing length follows the expected behaviour, i.e. $l = 0.41y$. In layer A the streamwise developments of l/δ appears to follow a behaviour which results from the combined effects of a relaxing alternating pressure gradient and divergence. The maximum response of both layers is at a distance of about $20\delta_0$, and further downstream the profiles remain almost self-similar, but have larger values than the unperturbed flow. As expected the non-dimensional profiles of eddy viscosity, which were presented by Saddoughi (1988), showed similar trends, but had larger variations than the l/δ profiles. It appears that eddy-viscosity type calculation methods, which use the concept that Reynolds shear stress is uniquely related to the normal gradient of the longitudinal mean velocity, and also use the local length and velocity scales to non-dimensionalize these quantities, will not be able to predict this flow in the outer layer.

Smits *et al.* (1979*a*) showed that around the mid-layer for the boundary layer in the cylinder-flare experiment, the asymptotic value of α_0 in the amplification factor for mixing length, $l/l_0 = 1+\alpha_0 e/(\partial U/\partial y)$ (see also Bradshaw 1974), was about 10. This is the value of α used for the effects of divergence in the amplification factor, $F = 1+\alpha e/(\partial U/\partial y)$, in the prediction method of Bradshaw & Unsworth (1974). Figure 18 shows the α_0 values at the mid-layers for the present investigations. The asymptotic value appears to be about 6, which is much lower than that obtained by Smits *et al.* But note that here, as well as for the cylinder-flare case, the lag effects were not taken into account.

In general, prediction methods use two different concepts – gradient-diffusion and bulk-convection hypotheses – to relate the turbulent transport, in the y-direction, of turbulent energy or Reynolds stress to the profile of turbulent energy or Reynolds stress (Bradshaw 1972). The former hypothesis assumes that the triple products tend to behave like the Reynolds-stress gradients (e.g. Daly & Harlow 1970; Hanjalic & Launder 1972), while in the latter one the assumption is that they behave like the Reynolds stresses (Townsend 1956; Bradshaw, Ferriss & Atwell 1967).

From the gradient-diffusion hypothesis, eddy diffusivities for turbulent kinetic energy, $\nu_q = -\overline{q^2v}/(\partial\overline{q^2}/\partial y)$, and shear stress, $\nu_\tau = -\overline{uv^2}/(\partial\overline{uv}/\partial y)$, can be defined. As is evident from these formulations, ν_q and ν_τ, unlike eddy viscosity (which is eddy diffusivity of momentum), are genuine turbulence parameters. In the kinetic theory of gases the condition for the validity of the gradient-diffusion concept is that the

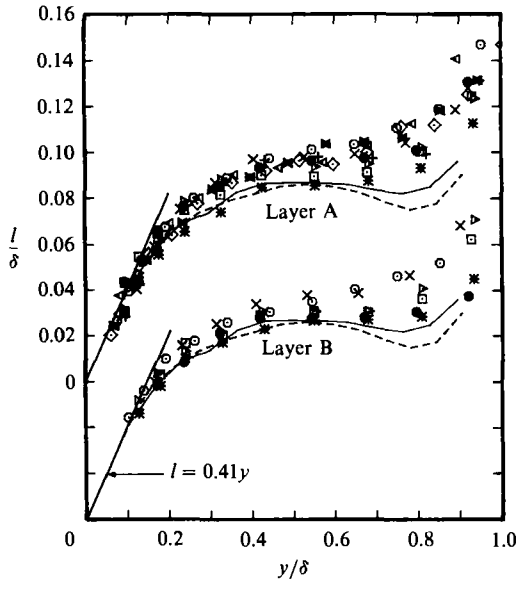

FIGURE 17. Profiles of mixing length, $l \equiv (-\overline{uv})^{\frac{1}{2}}/(\partial U/\partial y)$. For key to symbols see table 1 and figure 13.

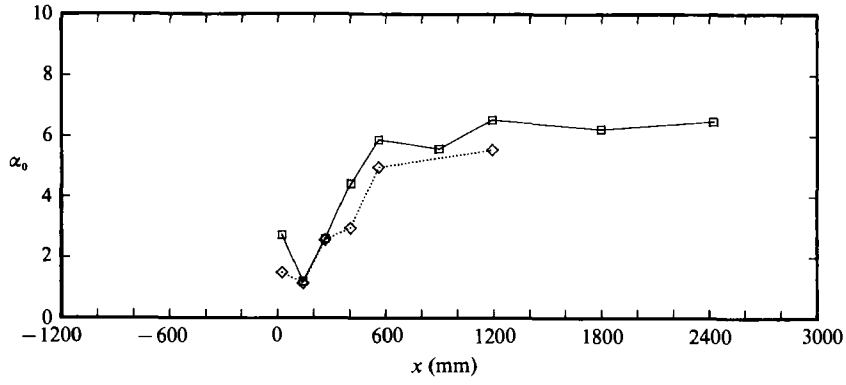

FIGURE 18. Streamwise development of amplification factor, α_0, at $y/\delta = 0.5$: ⊡, layer A; ◇, layer B.

mean free path shall be small compared with the flow width. Therefore the eddy diffusivities would be simply behaved only if the above condition is satisfied. This means that for turbulence which is dominated by large eddies, the gradient-diffusion formulation may be inappropriate (Muck *et al.* 1985). The profiles of non-dimensional eddy diffusivities, $\nu_q/(U_R\,\delta)$ and $\nu_\tau/(U_R\,\delta)$, are plotted in figure 19. These parameters in the diverging section are compared with those which were obtained at $R_\theta = 1196$ for a station in the straight section ($x = -410$) of layer A, since no other low-R_θ plane-flow data were available. In this plot, as well as the subsequent figure, it is assumed that $\overline{vw^2} = \frac{1}{2}(\overline{u^2v} + \overline{v^3})$ (Bradshaw 1967). In figure 19(*b*), the profiles of $\nu_\tau/(U_R\,\delta)$ are presented only for $y/\delta > 0.2$. This is because near the wall, while the triple products $-\overline{uv^2}$ have large values, a typical Reynolds-shear-stress profile shows roughly constant values of $-\overline{uv}$, so that the gradient $\partial\overline{uv}/\partial y$ tends to zero. As a result of this the eddy diffusivity, ν_τ, goes to infinitely large values, which implies a

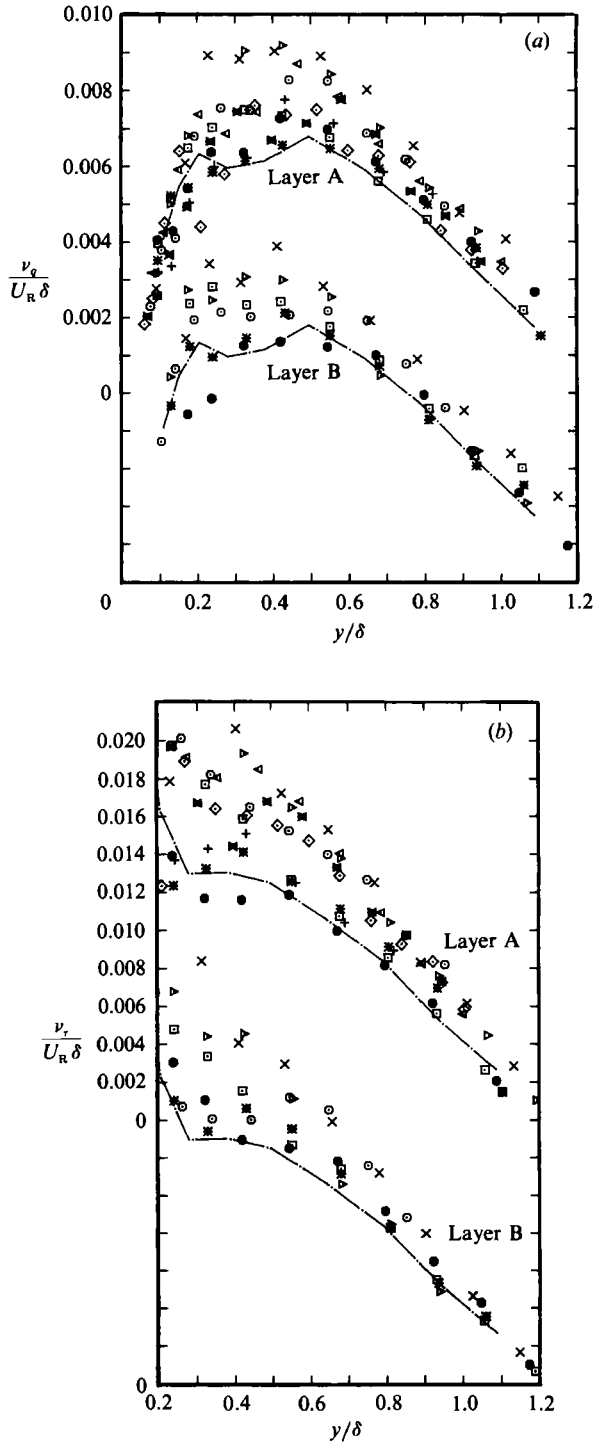

FIGURE 19. (*a*) Eddy diffusivity for turbulent kinetic energy, ν_q; (*b*) eddy diffusivisity for shear stress, ν_τ. —·—, $R_\theta = 1196$ ($x = -410$ mm) in the straight section of layer A. For key to other symbols see table 1.

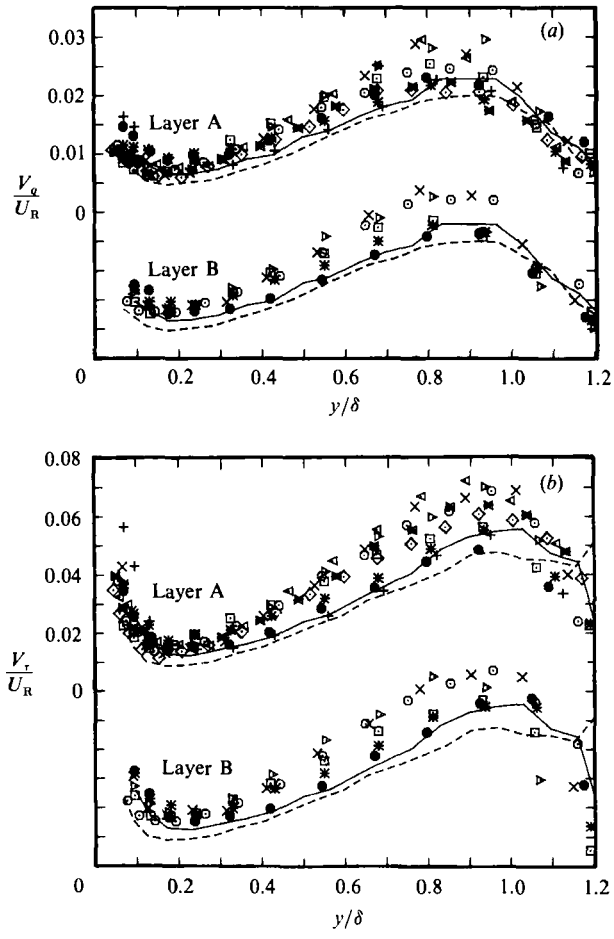

FIGURE 20. (*a*) Transport velocity of turbulent kinetic energy, V_q; (*b*) transport velocity of shear stress, V_τ. For key to symbols see table 1 and figure 13.

singularity in the gradient-diffusion parameter. As pointed out by Castro & Bradshaw (1976), eddy diffusivities necessarily have singularities because the triple products do not pass through zero at the same point as the stress gradient. In the present experiments for the range of y/δ where measurements were taken, no such singularity was observed in the eddy diffusivity for turbulent kinetic energy. As usual the values of these parameters for layer B are slightly lower than those for layer A. The streamwise developments of the eddy diffusivities are almost the same as those for the triple products. For example in the diverging section (layer B) around the mid-layer, the values of $(\nu_q/U_R\delta)$ and $(\nu_\tau/U_R\delta)$ increase with x up to about $x = 560$ and from then on they decrease. The substantial increase in their values, which in layer B is apparently due to the effects of divergence, is also somewhat like the raw triple products. Gibson, Verriopoulos & Vlachos (1984) showed that the eddy diffusitivites, ν_q and ν_τ, scaled on $\overline{(q^2 v^2)}/\epsilon$ (where ϵ is the dissipation) for both the flat and convex regions of their experiments. For the present investigations this type of scaling (not shown) indicated very large variations in the gradient-diffusion parameters at a given y/δ-position for the outer halves of the layers in the diverging section.

The bulk-convection hypothesis is used in the calculation method of Bradshaw *et al.* (1967). Here transport velocities in the y-direction, which represent the ensemble-average V-component velocities of large eddies (Smits *et al.* 1979*b*), are based on the assumption that turbulent transport is a pure convection by large eddies. This assumption is applicable only if the large eddies are weak (Bradshaw 1972). After neglecting the pressure-fluctuation part in the diffusion term, a turbulent transport velocity for turbulent kinetic energy is defined as $V_q = \overline{q^2 v}/\overline{q^2}$. Similarly, from the terms corresponding to the diffusion in the shear-stress balance equation, a turbulent transport velocity for shear stress, $V_\tau = \overline{uv^2}/\overline{uv}$, can be obtained. The profiles of V_q/U_R and V_τ/U_R are plotted in figure 20. In the region where the data were measured, the transport velocities were always positive, indicating that the transport of turbulent kinetic energy and shear stress is away from the wall. The rather large values near the wall are the direct consequence of the large values of triple products in this region. In layer A for the last stations, the values of V_q drop to those of the plane flow. V_τ profiles display some degree of self-similarity for the downstream stations, with an exception at the last station where the values reduce, but they still remain larger than plane-flow data at $R_\theta = 2180$. It appears that the transport velocities are better behaved than the eddy diffusivities.

The energy and shear-stress balance equations for the present experiments, as compared with the plane-flow case, contain extra production, $-(\overline{w^2} - \overline{v^2})\,\partial W/\partial z$, and generation, $(-\overline{uv})\,\partial W/\partial z$, terms respectively, which represent the explicit effect of lateral straining. The balances are presented by Saddoughi (1988), where the dissipation and redistribution were found by difference from their respective equations and the pressure diffusion was assumed to be small. Calculations of advection for the first and last stations are not possible, since the gradient of $\overline{q^2}$ with respect to x is present in this term. In layer A large values of advection occurred up to the station $x = 560$. The maximum value was at $x = 140$, which was a station in the adverse-pressure-gradient region. Since at $x = 140$ the production and diffusion were almost the same as those for the plane-flow data, these large advection values resulted in small values for dissipation in the outer layer. In this layer diffusion showed an increase at $x = 265$ ($\approx 10\delta_0$), and at $x = 895$ ($\approx 35\delta_0$) the values were still higher than the plane-flow data. Further downstream the values reduced. In layer B the differences between the diverging case and the plane-flow data reduced. The maximum advection and diffusion values occurred at $x = 265$ and 560 respectively. Contrary to the plane-flow data where, at the outer edge of the layer, diffusion and advection are approximately equal, for the present experiments it appeared that, in this part of each layer, the turbulent transport terms were larger than the mean-transport ones. The streamwise development of the transport terms of the shear-stress equation also closely followed the above trends.

Bradshaw, *et al.* (1967) defined a dissipation lengthscale as $L = (-\overline{uv})^{\frac{3}{2}}/\epsilon$. For a flow in energy equilibrium, L is equal to the mixing length. The values of dissipation obtained from the balances, which are known to have large uncertainties, were used to calculate the L profiles. The normalized values are shown in figure 21. Near the wall, L-values are nearly equal to the mixing length and the profiles follow the line $L = 0.41y$. In the outer layer, the L-values for the present experiments are larger than the plane-flow values and also the present-case mixing length. It should be noted that in the outer layer, the accuracy of the results depends on the accuracy of the advection. In layer A at $x = 140$, in the outer part of the boundary layer the L-values have increased by a large amount: the peak value is nearly twice that for the plane-flow case. This increase is the consequence of the very small dissipation which

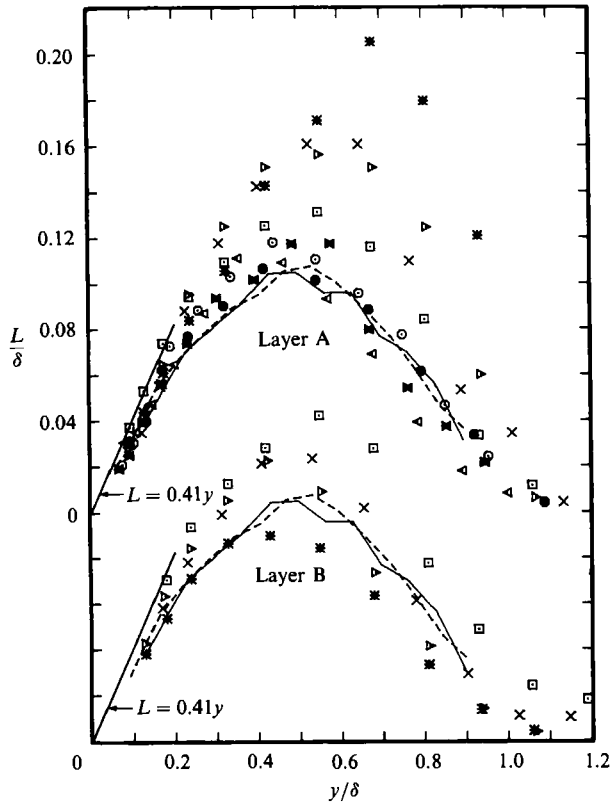

FIGURE 21. Profiles of dissipation lengthscale, $L = (-\overline{uv})^{1.5}/\epsilon$. For key to symbols see table 1 and figure 13.

resulted from the large advection values at this station. It is known that dissipation in the central part of a retarded boundary layer is very small (see Bradshaw 1967). In layer B for the same station, where the pressure gradient was smaller, the L values have decreased to almost the unperturbed values. This shows that the large increase in layer A at this station, cannot be totally attributed to the uncertainty in dissipation. Overall it appears that divergence tends to increase the values of the dissipation lengthscale and the maximum response in layer B, which represents the effects of divergence better than layer A, was at $x \approx 10\delta_0$.

To predict the rise in L at $x = 140$ for layer A, the present results show that in the calculation method of Bradshaw & Unsworth (1974) the unlagged value of α in the amplification factor for the dissipation lengthscale, $L/L_0 = 1 + \alpha e/(\partial U/\partial y)$, should be as high as 19. However, for layer B around the mid-layer at $x = 265$ ($\approx 10\delta_0$), as well as at 405 and 560, the data indicated an α-value of about 10, which is the value used for divergence effects in this prediction method.

Recently, Hunt, Spalart & Mansour (1987) proposed a model for the dissipation length in boundary layers, which is of the following form (see Cutler & Johnston 1989):

$$L = \left(\frac{-\overline{uv}}{\overline{v^2}}\right)^{\frac{3}{2}} \left(\frac{A_B}{y} + A_S \frac{\partial U/\partial y}{(\overline{v^2})^{\frac{1}{2}}}\right)^{-1}, \tag{5}$$

where $A_B = 0.27$ and $A_S = 0.46$. Using the above model with the present

measurements the dissipation lengthscales were calculated at all the stations for both layers. In layer A, this model underestimated the peak value at $x = 140$: the model predicted $L/\delta \approx 0.12$, but the value evaluated from the dissipation was about 0.2. For the points in layer B around the mid-layer at those stations for which the L profiles are shown in figure 21, after taking into account the large uncertainty in dissipation, the agreement with the model was very good.

3.2.3. *Some statistical properties*

Skewness, which is an odd-order moment of the probability density, gives an indication of the degree of asymmetry of distribution about the mean. The fourth moment or flatness is a measure of the width of the distribution. $S_u = \overline{u^3}/(\overline{u^2})^{\frac{3}{2}}$ and $F_u = \overline{u^4}/(\overline{u^2})^2$ are the u-component skewness and flatness factors respectively – similar definitions also apply for the v- and w- component velocity fluctuations. For a Gaussian process, skewness and flatness factors are zero and 3 respectively.

All the profiles of skewness and flatness factors for the present experiments are shown by Saddoughi (1988), where they have been compared with the plane-flow data. These profiles showed that the effects of divergence on the inner half of the boundary layers were very small since, as expected, in general the extra-strain-rate effects are felt mainly in the outer layers. It is known that for a two-dimensional mean flow S_w should be zero. Shiloh, Shivaprasad & Simpson (1981) found that their S_w values were slightly positive. They attributed this to the experimental uncertainty. For the present cases, S_w values for the major part of the layers also appeared to be slightly positive. Compared with the plane-flow data, the absolute values of the other skewness and flatness factors in the outer layers of the present investigation increased. For example see the profiles of S_v and F_u shown in figures 22 and 23 respectively. The profiles of S_v show a significant upward shift everywhere in the outer half of the layers, especially around the outer edges. For the present experiments, S_v reaches a maximum value of about 2.5, which is nearly equal to the maximum absolute value of S_u, whereas the plane-flow value of S_v is about 1.5. This more positive skewness has resulted from sharper positive spikes in the v-signal. It appears that S_v profiles, after the initial maximum response to divergence, become almost self-similar for the rest of the diverging section. The increase in the F_u values for the present layers for the region of $y/\delta > 0.6$ can be seen in figure 23, albeit these profiles apparently show some self-similarity beyond $x \approx 50\delta_0$. The increase in the entrainment rate and the higher-than-plane-flow values of the three flatness factors in the outer parts of the present layers, possibly, imply an increase in the extent of the intermittent region (Head & Patel 1968). However, this conclusion should be taken cautiously, since Kuo & Corrsin (1971) have stated that, 'although an intermittent variable is likely to have a high flatness factor, a high flatness factor does not necessarily imply intermittency'. This was shown by Muck *et al.* (1985), who found that after application of mild convex curvature, all three flatness factors decreased in the outer part of the layer, but intermittency measurements showed very small effects of curvature. The decrease in the flatness factor was shown by them to be the result of an increase in the ratio of fluctuation intensity in the free stream to that in the turbulent region (see also Wood & Bradshaw 1982 for an analytical treatment of the above).

3.3. *Spectra*

Spectra were taken at all the stations on the plane of symmetry of both layers, for the same y-positions where broadband-turbulence quantities were measured.

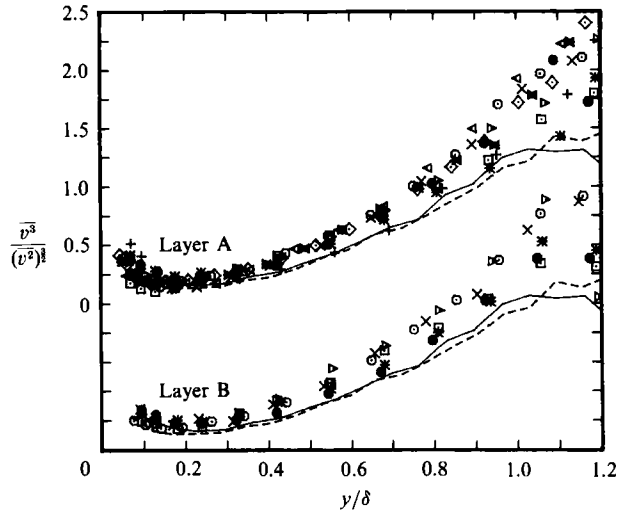

FIGURE 22. Profiles of v-component skewness factor, S_v. For key to symbols see table 1 and figure 13.

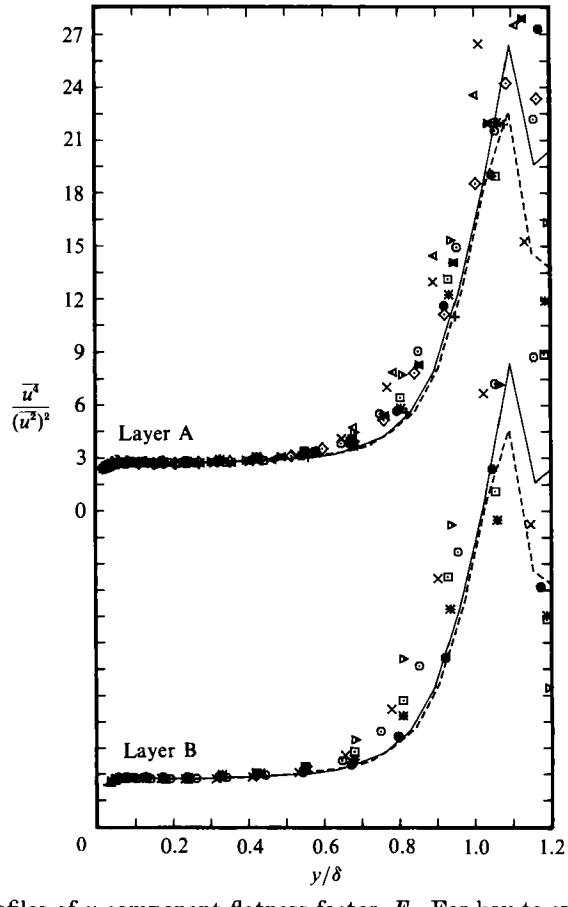

FIGURE 23. Profiles of u-component flatness factor, F_u. For key to symbols see table 1 and figure 13.

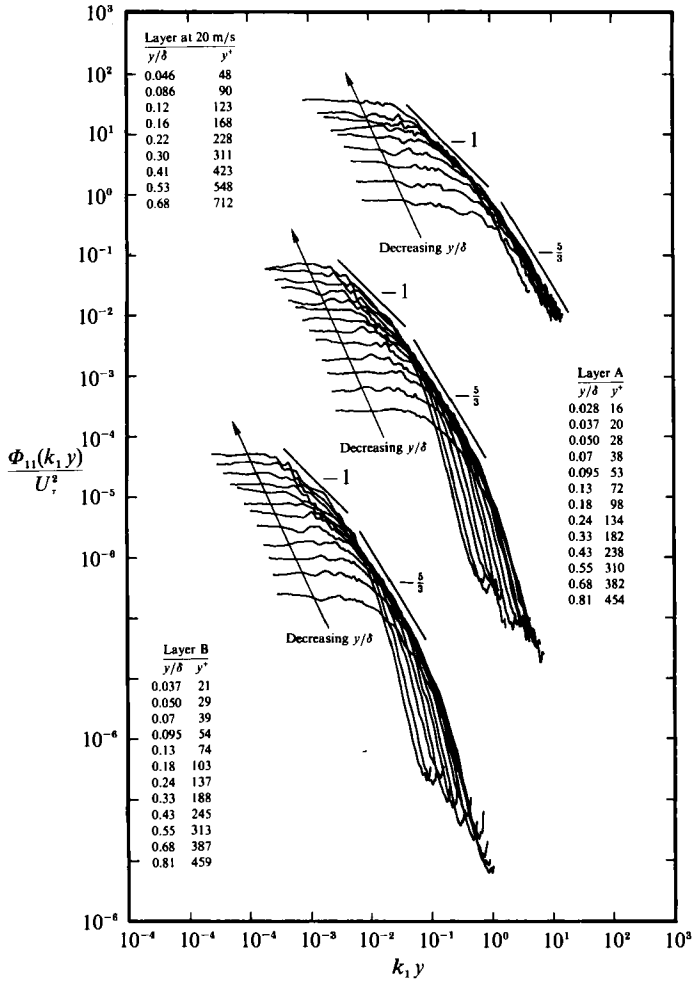

FIGURE 24. u-Spectra for varying values of y/δ at $x = 140$ mm for layer A, layer B and an additional family at 20 m/s. Inner-flow scaling.

Saddoughi (1988) presents the complete families of spectra for all the measurement stations. As an example of such plots, figure 24 shows the complete families of u-spectra for the station $x = 140$, plotted with the inner-flow scaling of Perry, Henbest & Chong (1986). In this figure, an additional family, which corresponds to a reference velocity of 20 m/s, is also shown. The diverging boundary layer for this case negotiated the same pressure gradients as layer A. The complete results for this layer are given by Saddoughi, Erm & Joubert (1985) and Saddoughi (1988). The behaviour of all the complete families of the spectra for u, v and w at low to moderate wavenumbers appeared to be consistent with Perry & Chong's (1982) and Perry *et al.*'s model, that is, for small values of y/δ an inverse-power-law region could be discerned for u- and w-spectra, whereas for the v-spectra at the same y/δ no such region was apparent, and all the spectra, except those for low values of y^+, for each layer at each station appeared to collapse to a $-\frac{5}{3}$ power-law region at high $k_1 y$, which is consistent with the classic $-\frac{5}{3}$ spectral law (Kolmogorov 1941). Since the present measurements are for low Reynolds numbers, the effects of viscosity in the

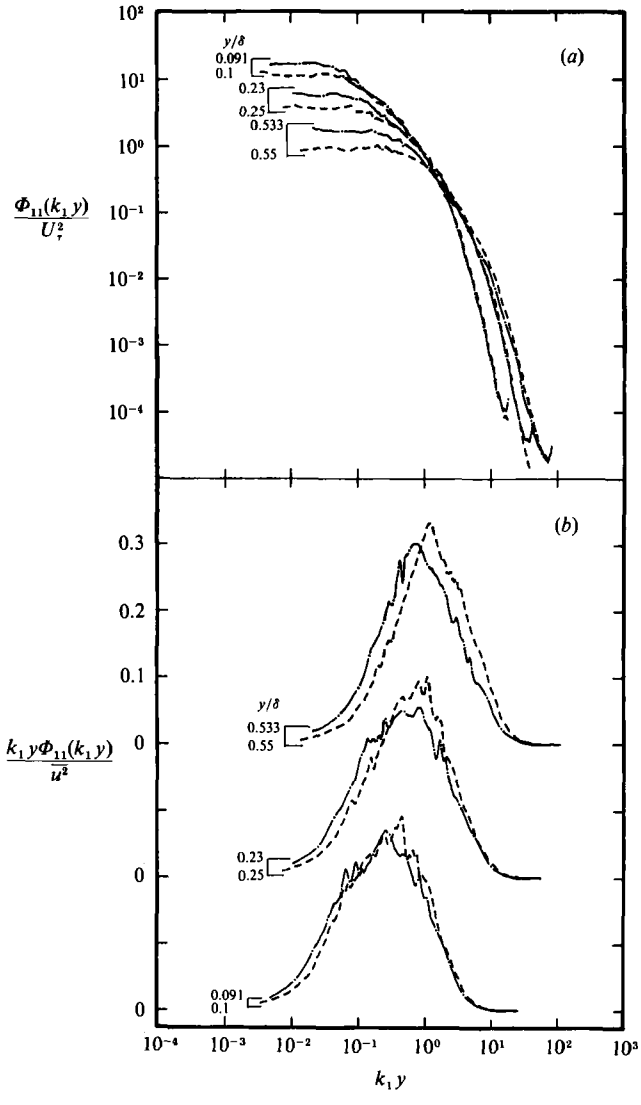

FIGURE 25. Comparisons for u-spectra for layer A ($x = 560$ mm, $R_\theta = 1389$, dash-dot line) with those for Erm (1988) ($R_\theta = 1565$, dashed line) showing the effects of divergence at fixed values of y/δ: (*a*) log–log plot; (*b*) pre-multiplied plot.

higher-wavenumber region are more significant than for high-Reynolds-number flows. According to Perry *et al.*, the spectra peel off from the inertial subrange at decreasing values of $k_1 y$ as y/δ decreases for a fixed Reynolds number, so that a $-\frac{5}{3}$ power-law region evolves into a $-\frac{5}{3}$ power-law envelope at low Reynolds numbers. In figure 24, this behaviour can be clearly seen for the spectra for layers A and B, which are at lower Reynolds number than the layer at 20 m/s.

To identify the effects of divergence, the u-spectra at selected values of y/δ for layer B at the measurement station $x = 560$ are compared in figure 25 with the plane-flow data which are nominally at the same y/δ and R_θ as the present case. While part (*a*) shows the log-log plot, part (*b*) represents the same data plotted in a pre-multiplied form such that the area under each spectrum is equal to unity. As a result

of the effects of divergence, the energy-containing parts of the pre-multiplied spectra in the outer layer of the present case appear to be slightly broadened and shifted towards lower wavenumbers. Hence, the increase in the $\overline{u^2}$ Reynolds stress may be attributed to the increased energy in low-wavenumber, large-scale motions. It appears that the other extra-strain rates also affect the low-wavenumber region in the spectra (see Hunt & Joubert 1979; Watmuff, Witt & Joubert 1985; Barlow & Johnston 1988).

4. General discussion and concluding remarks

The experimental studies undertaken here were concerned mainly with one aspect of complex flows: the streamline divergence. The literature survey revealed that hitherto no thorough investigation of the effects of this extra-strain rate on turbulent boundary layers had been documented. Detailed hot-wire measurements for the planes of symmetry of two layers – layers A and B – have been presented. These two layers had the same (low) Reynolds number, and both were developed in the presence of the same amount of prolonged ($\approx 100\delta_0$) simple divergence with a maximum divergence parameter of about 0.075, but the (mild) pressure-gradient parameter for the upstream region of layer B was about half of that for layer A.

Although one could not define clear-cut regions of response, it appeared that two overlapping stages of development were involved. The initial stage covered a distance of about 20 to $25\delta_0$. In this region the coupled effects of pressure gradient and divergence were present, and the boundary-layer properties changed rapidly. Some of the mean-flow quantities, such as δ, θ and R_θ (≈ 1400), responded almost immediately to the application of divergence, and remained constant for the entire length of this region, despite the fairly large reduction in divergence parameter. The other parameters, like skin-friction coefficient, wake parameter and entrainment rate, which are known to be sensitive to even small pressure gradients, changed quickly within a distance of $10\delta_0$. Further downstream, as a response to divergence, C_f and C_{E} increased up to the end of the first region, but Π reached its minimum value around $35\delta_0$. In the inner layer, the Reynolds stresses responded quickly to pressure gradients and the effects of the change-in-pressure-gradient jump propagated slowly outward towards the outer layer (see e.g. Smits & Wood 1985; Bradshaw & Ferris 1965). This process was completed by the end of the first region. The stresses in the outer layer did not increase significantly, which is contrary to the expectation that one would have had from the destabilizing effects of large divergence. In the outer layer a peak was developed on the triple products, which moved towards the centre of the layer, and at the end of the first region the value of the peak had nearly doubled. If this outward-progressing peak resulted from the development of large-eddy eruptions (Smits *et al.* 1979*a*), this process was also completed by the distance of 20 to $25\delta_0$, since further downstream the position of the peak did not change. The maximum response of mixing length was also at the end of the first region, but the dissipation lengthscale had a peak value nearly twice that of the plane-flow case at $5\delta_0$, as a response to adverse pressure gradient. The maximum response of this parameter to divergence was at about $10\delta_0$.

In the second region, which lasted for almost the rest of the diverging section, the pressure-gradient effects were negligible and also the rate of decrease in divergence parameter was very small. Here, although R_θ increased gradually, till the last measurement station the flow was considered to be low Reynolds number, since at

this station R_θ was only about 2000. In this region C_f, Reynolds stresses the triple products decreased slowly, owing to the increase in R_θ (Murlis *et al* 1982; Erm 1988). At the last station, the Reynolds shear stresses dropped back to the plane-flow data of Erm for $R_\theta = 2180$, but the normal stresses were slightly larger than those corresponding to the plane-flow case. Also, the peak in the triple products at this station was much higher than the plane-flow data, but the position of the peak in the layer had not changed. In this second region of development beyond $x \approx 35\delta_0$ the wake parameter, which had a very low value, became nearly constant and independent of R_θ. This apparently indicated that the boundary layer had reached a state of equilibrium and possibly the wake parameter was correlated with the rate of strain due to divergence (V. C. Patel, private communication). On the other hand, the entrainment rate had a delayed response and attained a constant value at around $50\delta_0$. The mixing-length profiles, which had increased in the first region, retained their high values and were self-similar for almost the entire length of the second region. The transport velocities appeared to have delayed maximum responses (increase), which occurred in the second region at about $35\delta_0$. Further downstream, the transport velocity for kinetic energy reduced and for the last station nearly collapsed onto the plane-flow data, but the transport velocity for shear stress only decreased very gradually. Possibly one could consider that the profiles of V_τ also showed some degree of self-similarity, except for the last station. However, the state of equilibrium of the boundary layer for $x > 35\delta_0$, could be clearly seen in the profiles of v-skewness factor. The profiles of flatness factors appeared to become self-similar only beyond $50\delta_0$.

The present results give further indications that the boundary-layer response to the prolonged application of an extra-strain rate is a complex process and certainly we do not pretend to have understood all the physical aspects involved in this process but, in comparison with the plane-flow case, one may suggest the following explanation of the data. After prolonged application of divergence, the boundary layer appears to have reached a state of equilibrium. In this state the increase in flatness factors around the outer edge of the layer and also the increase in the entrainment rate might have been due to an increase in the extent of the intermittent region (Head & Patel 1968). There is more (nearly double the plane-flow case) positive v-skewness, which has resulted from sharper positive spikes in the v-signal. The turbulent transport of kinetic energy ($\overline{q^2 v}$) and shear stress ($\overline{uv^2}$) by the v-fluctuations have increased, which in turn have enhanced the magnitude of the diffusion in the outer layer. Hence there has been an increase in turbulent mixing, which has produced a reduction in mean-velocity gradient ($\partial U/\partial y$) and therefore a large reduction in the wake parameter (Ramaprian & Shivaprasad 1978; Hoffmann *et al.* 1985). Also, it is this reduction in $\partial U/\partial y$ which is partly responsible for the eddy viscosity maintaining its larger-than-standard value at the downstream stations, even though the Reynolds shear stresses have reduced to the plane-flow values. Overall, it appears that divergence significantly enhances the process of turbulent diffusion, but not the production of turbulent energy in the boundary layer. Thus the triple correlations have to be modelled appropriately. However, the increase in turbulent mixing has not been sufficient to affect the dimensionless structure parameters, since for the entire flow they showed only negligible deviations from the unperturbed values, which is opposite to the findings of Smits *et al.* (1979*a*) who concluded that divergence altered these parameters in the same way as longitudinal curvature. The current results perhaps indicate that the perturbations in the present investigation have resulted in mainly a quantitative amplification (for the first

region) or reduction (for the second region) in intensity rather than a qualitative change in large-eddy configurations (Muck *et al.* 1985). This is an encouraging sign for those turbulence models which assume a constant value for each of these parameters.

The calculation method of Bradshaw & Unsworth (1974) and the model of Hunt *et al.* (1987) predicted the values of dissipation length scale very well for the region where divergence alone was present, but both these methods underestimated the peak value of this parameter at $x = 140$. The spectral results, which were plotted using the inner-flow scaling of Perry *et al.* (1986), showed that divergence mainly affected the low-wavenumber, large-scale motions.

This project was financially supported by the Australian Research Council. We are grateful to Dr L. P. Erm for his help and support. The authors would also like to thank Professor P. Bradshaw of Stanford University and Professor V. C. Patel of the University of Iowa for their encouragements and helpful comments, when they examined the Doctoral-thesis version of this paper.

REFERENCES

ALVING, A. E., SMITS, A. J. & WATMUFF, J. H. 1990 *J. Fluid Mech.* **211**, 529.

BARLOW, R. S. & JOHNSTON, J. P. 1988 *J. Fluid Mech.* **191**, 137.

BRADSHAW, P. 1967 *J. Fluid Mech.* **29**, 625.

BRADSHAW, P. 1971 *AGARD Conf.* **30**, 241.

BRADSHAW, P. 1972 *Aero. J.* **76**, 403.

BRADSHAW, P. 1973 *AGARDograph* **169**.

BRADSHAW, P. 1974 *J. Fluid Mech.* **63**, 449.

BRADSHAW, P. 1988 Effects of extra rates of strain – review. *Zoran Zaric Memorial Sem., Dubrovnik.* Hemisphere.

BRADSHAW, P. & FERRISS, D. H. 1965 *NPL Aero. Rep.* 1145.

BRADSHAW, P., FERRISS, D. H. & ATWELL, N. P. 1967 *J. Fluid Mech.* **28**, 593.

BRADSHAW, P. & UNSWORTH, K. 1974 *I.C. Aero. Rep.* 74-02.

BREDERODE, V. DE & BRADSHAW, P. 1974 *I.C. Aero. Rep.* 74-03.

CASTRO, I. P. & BRADSHAW, P. 1976 *J. Fluid Mech.* **73**, 165.

CEBECI, T. & SMITH, A. M. O. 1974 *Analysis of Turbulent Boundary Layers.* Academic.

COLES, D. E. 1962 *Rand Rep.* R-403-PR.

CRABBE, R. S. 1977 A contribution to the study of uniformly diverging and converging turbulent boundary layers. Ph.D. dissertation, Mech. Engng, McGill University.

CUTLER, A. D. & JOHNSTON, J. P. 1989 *J. Fluid Mech.* **200**, 367.

DALY, B. J. & HARLOW, F. H. 1970 *Phys. Fluids* **13**, 2634.

ERM, L. P. 1988 Low Reynolds number turbulent boundary layers. Ph.D. thesis, Mech. Engng, University of Melbourne.

GALBRAITH, R. A. M. & HEAD, M. R. 1975 *Aero. Q.* **26**, 133.

GIBSON, M. M., VERRIOPOULOS, C. A. & VLACHOS, N. S. 1984 *Expts Fluids* **2**, 17.

GILLIS, J. C. & JOHNSTON, J. P. 1983 *J. Fluid Mech.* **135**, 123.

HANJALIC, K. & LAUNDER, B. E. 1972 *J. Fluid Mech.* **52**, 609.

HEAD, M. R. 1958 *Aero. Res. Counc. R&M* 3152.

HEAD, M. R. 1976 *Aero. Q.* **27**, 270.

HEAD, M. R. & PATEL, V. C. 1968 *Aero. Res. Counc. R&M* 3643.

HEAD, M. R. & PRAHLAD, T. S. 1974 *Aero. Q.* **25**, 293.

HOFFMANN, P. H., MUCK, K. C. & BRADSHAW, P. 1985 *J. Fluid Mech.* **161**, 371.

HUNT, I. A. & JOUBERT, P. N. 1979 *J. Fluid Mech.* **91**, 633.

HUNT, J. C. R., SPALART, P. R. & MANSOUR, N. N. 1987 *Proc. Summer Prog., Center for Turbulence Research*, Stanford.

INMAN, P. N. & BRADSHAW, P. 1981 *AIAA J.* **19**, 653.

KEHL, A. 1943 *Ing. Archiv.* **13**, 293.

KOLMOGOROV, A. N. 1941 *C.R. Acad. Sci. URSS* **30**, 301.

KUO, A. Y. & CORRSIN, S. 1971 *J. Fluid Mech.* **50**, 285.

LIGRANI, P. M. & BRADSHAW, P. 1987 *Expts Fluids* **5**, 407.

MEHTA, R. D. & BRADSHAW, P. 1979 *Aero. J.* 433.

MUCK, K. C., HOFFMANN, P. H. & BRADSHAW, P. 1985 *J. Fluid Mech.* **161**, 347.

MURLIS, J. 1975 The structure of a turbulent boundary layer at low Reynolds number. Ph.D. thesis, Imperial College, London.

MURLIS, J., TSAI, H. M. & BRADSHAW, P. 1982 *J. Fluid Mech.* **122**, 13.

PATEL, V. C. 1965 *J. Fluid Mech.* **23**, 185.

PATEL, V. C. & BAEK, J. H. 1987 *AIAA. J.* **25**, 550.

PATEL, V. C., NAKAYAMA, A. & DAMIAN, R. 1974 *J. Fluid Mech.* **63**, 345.

PERRY, A. E. 1982 *Hot-Wire Anemometry*. Oxford University Press.

PERRY, A. E. & CHONG, M. S. 1982 *J. Fluid Mech.* **119**, 173.

PERRY, A. E., HENBEST, S. & CHONG, M. S. 1986 *J. Fluid Mech.* **165**, 163.

PERRY, A. E., LIM, K. L. & HENBEST, S. M. 1987 *J. Fluid Mech.* **177**, 437.

RAMAPRIAN, B. R. & SHIVAPRASAD, B. G. 1987 *J. Fluid Mech.* **85**, 273.

SADDOUGHI, S. G. 1988 Experimental studies of the effects of streamline divergence on developing turbulent boundary layers. Ph.D. thesis, Mech. Engng, University of Melbourne.

SADDOUGHI, S. G. 1989 Some selected contributions from Peter N. Joubert and his students to the study of perturbed turbulent boundary layers. *10th Australasian Fluid Mech. Conf. University of Melbourne*.

SADDOUGHI, S. G., ERM, L. P. & JOUBERT, P. N. 1985 The effects of streamline divergence on developing turbulent boundary layers. *Proc. Osaka Intl Colloq. Ship Visc. Flow*, p. 11. Osaka University and University of Osaka Prefecture, Japan.

SHILOH, K., SHIVAPRASAD, B. G. & SIMPSON, R. L. 1981 *J. Fluid Mech.* **113**, 75.

SJOLANDER, S. A. 1980 Eddy viscosity in two-dimensional and laterally strained boundary layers. Ph.D. dissertation, University of Cambridge.

SMITS, A. J., EATON, J. A. & BRADSHAW, P. 1979*a* *J. Fluid Mech.* **94**, 243.

SMITS, A. J. & JOUBERT, P. N. 1982 *J. Ship Res.* **26**, 135.

SMITS, A. J. & WOOD, D. H. 1985 *Ann. Rev. Fluid Mech.* **17**, 312.

SMITS, A. J., YOUNG, S. T. B. & BRADSHAW, P. 1979*b* *J. Fluid Mech.* **94**, 209.

TOWNSEND, A. A. 1956 *The Structure of Turbulent Shear Flow*. Cambridge University Press.

WATMUFF, J. H., WITT, H. T. & JOUBERT, P. N. 1985 *J. Fluid Mech.* **157**, 405.

WILLMARTH, W. W. & BOGAR, J. B. 1977 *Phys. Fluids Suppl.* **20**, S9.

WILLMARTH, W. W. & SHARMA, L. K. 1984 *J. Fluid Mech.* **142**, 121.

WOOD, D. H. & BRADSHAW, P. 1982 *J. Fluid Mech.* **122**, 57.